Politecnico di Torino

Politecnico di Torino

Energy and nuclear engineering
Academic Year 2024/2025
Graduation Session July 2025

Modelling of the Vacuum Pumping system and integration in the Fuel Cycle of a nuclear fusion power plant

Advisors:
Dr. Samuele Meschini
Prof. Raffaella Testoni
Prof. Massimo Zucchetti

Candidate:
Riccardo Manfredi Selvaggi

Abstract

Nuclear fusion represents a promising solution for sustainable and large-scale energy production, with tritium playing a central role as a key fuel. Efficient tritium management, including its breeding, recovery, and recycling, is essential to ensure the viability of a fusion power plant, and is governed by the design and performance of the fuel cycle system.

Existing models of the nuclear fusion fuel cycle often rely on simplified assumptions, such as the use of residence time to describe the behaviour of gas retention. While computationally efficient, these models lack a detailed description of the physical processes governing the system and offer limited insight into the operation and limitations of key components. A detailed modelling of the exhaust gas pumping system can instead provide critical information regarding tritium burning efficiency, fuel cycle dynamics, and the estimation of the reactor's startup tritium inventory.

In this thesis, a detailed model of the vacuum pumping system was developed, including both cryopumps and vapor diffusion pumps. The work builds upon a fuel cycle model developed at the MIT Plasma Science and Fusion Center (PSFC) and Politecncico di Torino, extending it with a more detailed and physically accurate description of exhaust processes. One of the major improvements introduced was the inclusion of surface saturation effects: condensation and absorption limitations were implemented to reflect the finite capacity of cryogenic surfaces. The pumping speed was characterized dynamically as a function of surface loading, allowing the model to capture the physical behaviour of the pumps over time more realistically. This time-dependent degradation of pumping performance is essential to understand when evaluating the operational efficiency and regeneration requirements of the system.
Furthermore, the model takes into account safety-critical aspects such as the risk of hydrogen accumulation and explosion inside the pumping chamber, a particularly important consideration in hydrogen-handling environments. The result is a simulation framework that significantly enhances state-of-the-art modelling approaches, providing deeper physical insight and predictive capability for the design and optimization of first-generation fusion power plant fuel cycles.

Table of Contents

Chapter 1 - Description of the Fuel Cycle model

Nuclear fusion is one of the most promising solutions to the global energy demand. Fusion reactions involve the combination of light atomic nuclei to form heavier nuclei, releasing a significant amount of energy in the process. Among the various reactions studied for energy production, the deuterium-tritium (D-T) reaction is the most favorable due to its high cross-section at relatively low temperatures (~10 keV), making it the leading candidate for early fusion reactors.

During this process, a deuterium nucleus (^{2}H) and a tritium nucleus (^{3}H) unite to form a helium-4 nucleus and a fast neutron, releasing the total energy of 17.6 MeV. Deuterium is easily found and can be extracted from water, but tritium is a radioactive isotope with half-life ~12.3 years and is not found in nature in significant quantities. To this end, tritium must be bred within the reactor itself through neutron reactions with lithium, typically in a breeding blanket around the plasma. This necessity establishes the tritium fuel cycle. The fuel cycle encompasses all the operations that tritium participates in, from production in the breeding blanket, extraction, purification, storage, injection into the plasma, and finally exhaust gas processing and recycling.

The Fuel Cycle (FC) model used in this work is based on the one described in [1], developed for an ARC-like reactor at the MIT Plasma Science and Fusion Center (PSFC) and Politecnico di Torino. In its original formulation, each component of the cycle, including the Vacuum Pumping (VP) system, was represented using a lumped-parameter approach based on the Residence Time Method (RTM). This method simplifies the behaviour of each subsystem by characterizing gas retention and flow through characteristic time constants. The time evolution of tritium inventories across the system is governed by a set of ordinary differential equations (ODEs), which track the tritium mass balance dynamically.

In this thesis, the VP component was reformulated with a more physically accurate model and then reintegrated into two versions of the Fuel Cycle: a simplified version including only the essential components, and the full version encompassing the entire tritium management system. Both configurations are presented in this chapter, as shown in Figure 1.

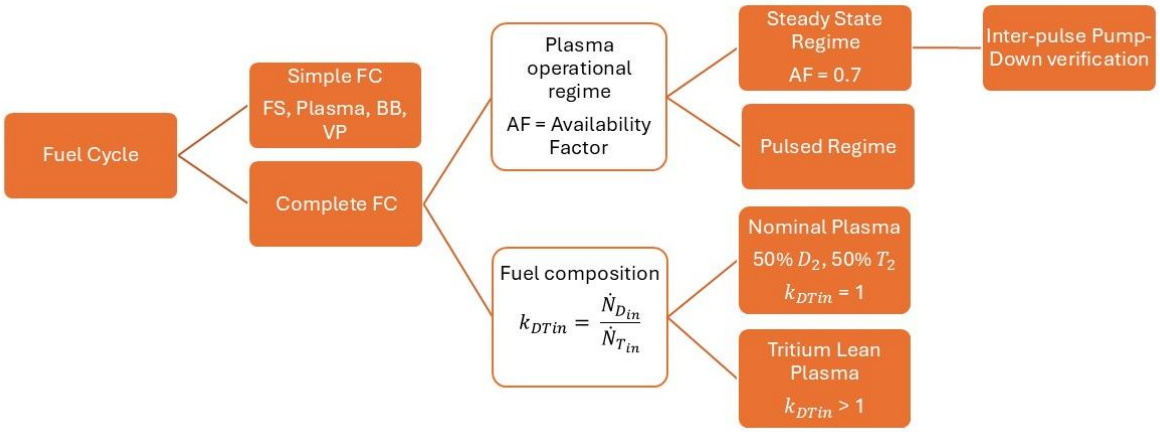

Figure 1 - Fuel Cycle complexity tree diagram adopted in this work

1.1 Essential components of a simple Fuel Cycle

A simplified model of the Fuel Cycle in a nuclear fusion power plant includes four essential components, each playing a distinct role in the management and conservation of tritium. These components interact to ensure tritium is efficiently injected, used, recovered, and regenerated within the system. Their key functions in the tritium economy are summarized below:

- Storage and Fuelling System injects a tritium flow rate $\dot{N}_T^{in}\ [Kg \cdot s^{-1}]$ into the vacuum chamber. In this work it's assumed that the tritium flow rate is constant, although time-dependent flow rates can be modelled as well.
- Plasma: within the vacuum chamber, a fraction of the injected tritium undergoes fusion reactions. Tritium Burning Efficiency is defined as:

$$\text{TBE} = \frac{\dot{N}_T^{burn}}{\dot{N}_T^{in}}$$

- Vacuum Pumping: the unburned tritium is exhausted through the divertor and extracted by the vacuum pumps, which return it to the fuelling system. The exhausted flows is:

$$\dot{N}_T^{div} = \dot{N}_T^{in} - \dot{N}_T^{burn} = \dot{N}_T^{in}(1 - TBE)$$

- The Breeding Blanket generates tritium through nuclear reactions neutron-lithium interactions:

$$^{6}_{3}Li + n \rightarrow {}^{4}_{2}He + {}^{3}_{1}T + 4.8\ \text{MeV}$$
$$^{7}_{3}Li + n \rightarrow {}^{4}_{2}He + {}^{3}_{1}T + n - 2.5\ \text{MeV}$$

The Tritium Breeding Ratio (TBR) measures the tritium production relative to what is consumed by fusion:

$$TBR = \frac{\dot{N}_T^{source}}{\dot{N}_T^{burn}}$$

Tritium production must not only compensate for the tritium burned and lost (e.g., through radioactive decay or system inefficiencies), but also provide a surplus to support start-up inventories for future fusion reactors.

The required Tritium Breeding Ratio ($\mathrm{TBR_r}$) is the minimum TBR required to achieve tritium self-sufficiency, accounting for usage, radioactive decay, and extraction losses. So, a necessary condition is $\mathrm{TBR} > \mathrm{TBR_r} > 1$.

In the Figure 2, the interactions between the main Fuel Cycle components are illustrated. The diagram highlights the direct internal recycling loop from the Vacuum Pumping (VP) system back to the Fuelling System, as well as the tritium production from the Breeding Blanket, which supplies fresh fuel to the cycle.

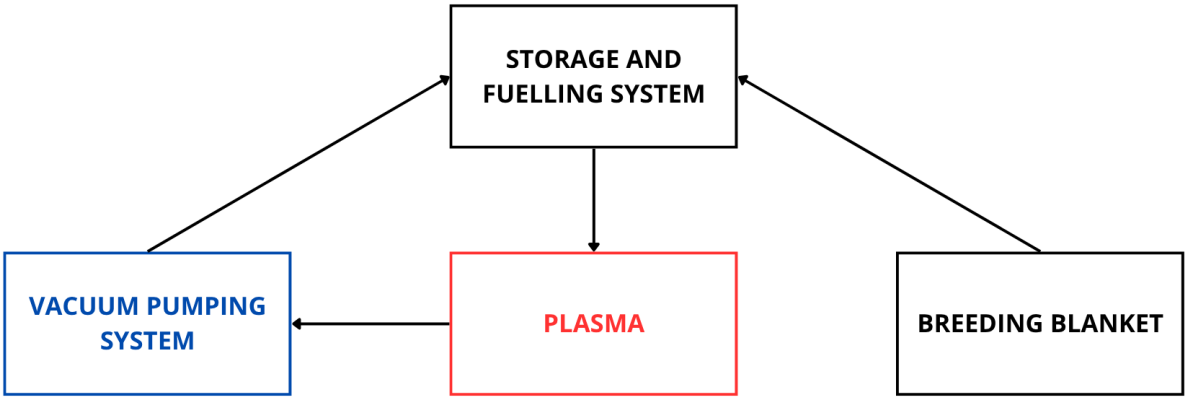

Figure 2 - Schematic representation of the main Fuel Cycle components and their interconnections, illustrating the exchange of tritium between subsystems. Arrows indicate the direction of tritium mass transfer.

1.2 Complete Fuel Cycle

The presence of tritium in each component of the fuel cycle is modelled using the residence time method, which allows for a simplified yet effective representation of tritium retention and transport within the system. In this approach, each component is treated as a well-mixed volume where tritium enters, is temporarily stored, and then exits according to a characteristic residence time.

The temporal evolution of the tritium inventory within a component is governed by a first-order differential equation which links the input flow rate, the internal accumulation, and the output flow rate.

$$\frac{dI_i}{dt} = \sum_{j \neq i} \left(f_{i \to j} \frac{I_j}{\tau_j} \right) - (1 - \epsilon_i) \left(\frac{I_i}{\tau_i} \right) - \lambda I_i + S_i$$

With initial conditions:

$$I_i(t = 0) = 0, \forall i \neq storage$$

$$I_{storage}(t = 0) = I_{startup}$$

Subscripts i and j refer to the generic ith and jth component, I is tritium inventory, τ is the residence time, λ is the tritium decay rate, and ϵ is the fraction of tritium lost due to non-radioactive phenomena (e.g. leakages).

Schematic representation of the complete FC is shown in Figure 3.

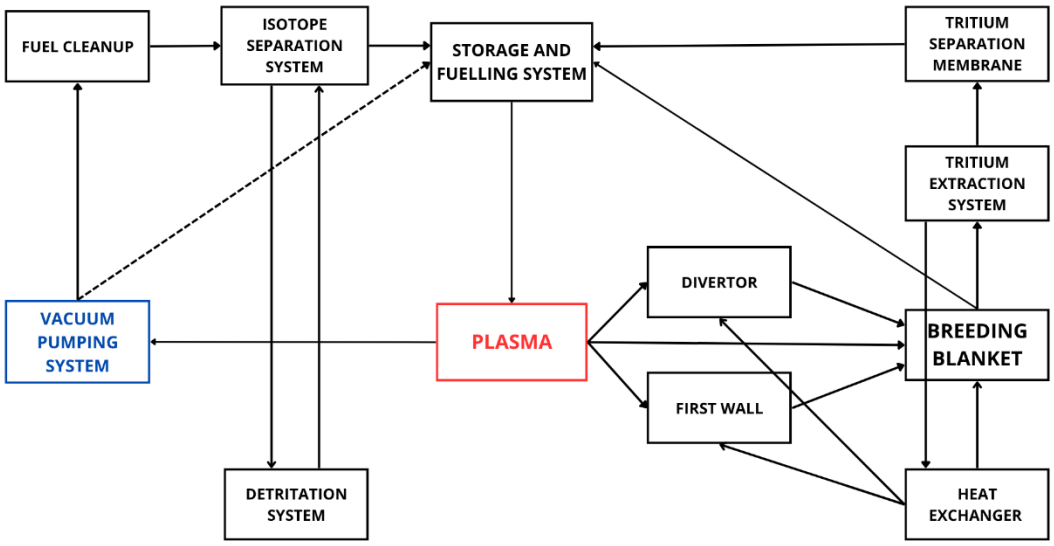

Figure 3 - Schematic representation of an ARC-class tokamak, equipped with a Liquid immersion Blanket (LiB), Fuel Cycle components and their interconnections, illustrating the exchange of tritium between subsystems. Arrows indicate the direction of tritium mass transfer. Dotter arrow indicates the Direct Internal Recycling.

Each component is assigned a specific average residence time, reflecting its characteristic retention capacity and flow dynamics. These values, summarized in Table 1, are based on experimental data or design estimates and play a key role in determining the time-dependent distribution of tritium within the entire fuel cycle.

In Table 1 is a detailed overview of additional subsystems that complete the Fuel Cycle in a D-T fusion power plant. These components play essential roles in tritium recovery, separation, purification, safety, and heat management.

Table 1 - Additional FC components, their functions and residence time

Component	Function	Residence time τ
First Wall FW	The plasma-facing surface of the reactor chamber. Tritium can be trapped by implantation or diffusion into structural materials and must be tracked for inventory control.	$1000s$
Divertor DIV	Extracts unburned fuel, helium ash, and impurities from the plasma edge. High heat and particle flux make it a critical zone for tritium exhaust and retention phenomena.	$1000s$

Fuel Cleanup System	Removes non-hydrogenic impurities (e.g., helium, nitrogen, water vapor) from the gas stream exiting the vacuum system before tritium reprocessing.	1h
Tritium Extraction System TES	Recovers tritium bred in the blanket or coolant loop (e.g., via helium purge or liquid PbLi extraction), enabling its reintegration into the fuel cycle.	24h
Heat Exchanger HX	Transfers thermal energy coolant, which is also the tritium carrier, to secondary circuits Ensures thermal control while avoiding tritium permeation or cross-contamination.	1h
Detritation System	Captures and recycles tritium from contaminated gaseous streams, leaks, or gloveboxes. Essential for safety and environmental protection.	1h
Isotope Separation System	Separates hydrogen isotopes (H_2, D_2, T_2) to allow high-purity tritium fuel to be reinjected. Techniques include cryogenic distillation columns or palladium membrane separation.	3h
Membrane	Allow selective permeation of hydrogen isotopes under pressure and temperature gradients. Can be used for both purification and tritium extraction from liquid metals or gas streams.	100s

Results of the complete Fuel Cycle simulations, showing tritium inventories [Kg] in the components during a 2 years simulation, are shown in Section 1.3. The end of the simulation time is set to be equal to the target doubling time, hence the time needed to double up the initial inventory in the fuelling system. In this simulation the VP is modeled with a residence time of 600s. It has to be considered the starting point of this work. Then, when the VP is going to be substitute with the new physics-based component, similar results are expected.

1.3 Tritium inventories and doubling time

The output of the fuel cycle model serves as the starting point for this work. The code can calculate the required tritium startup inventory $I_{startup}$ and the corresponding doubling time t_d for the reactor, which we assume operating at a fusion power of 500 MW. These calculations are performed based on a given tritium burn efficiency TBE.

Figure 4 shows the evolution of tritium inventories across various components of the ARC reactor's fuel cycle, assuming a Tritium Burn-up Efficiency of 0.02. It can be observed that the tritium inventory in the storage system approximately doubles over a two-year period. This behaviour is consistent with the assumptions used in the simulation, in which the Tritium Breeding Ratio (TBR) in the breeding blanket is set to 1.073—sufficient to achieve the target doubling time.

The doubling time t_d is defined as the time required to double the initial tritium inventory in the storage system. The excess tritium produced is assumed to be allocated for the startup of additional fusion reactors. A commonly accepted and ambitious goal for future power plants is a doubling time of approximately two years.

In this simulation, reported in Figure 4, the required initial tritium inventory was calculated to be $I_{startup}$ = 1.37 kg, and the resulting doubling time was found to be t_d = 1.88 y, thereby fulfilling the design target.

In Section 4.8 Tritium inventory in the FC, it will be shown that similar outcomes are obtained when the vacuum pumping (VP) component is replaced with the more detailed model.

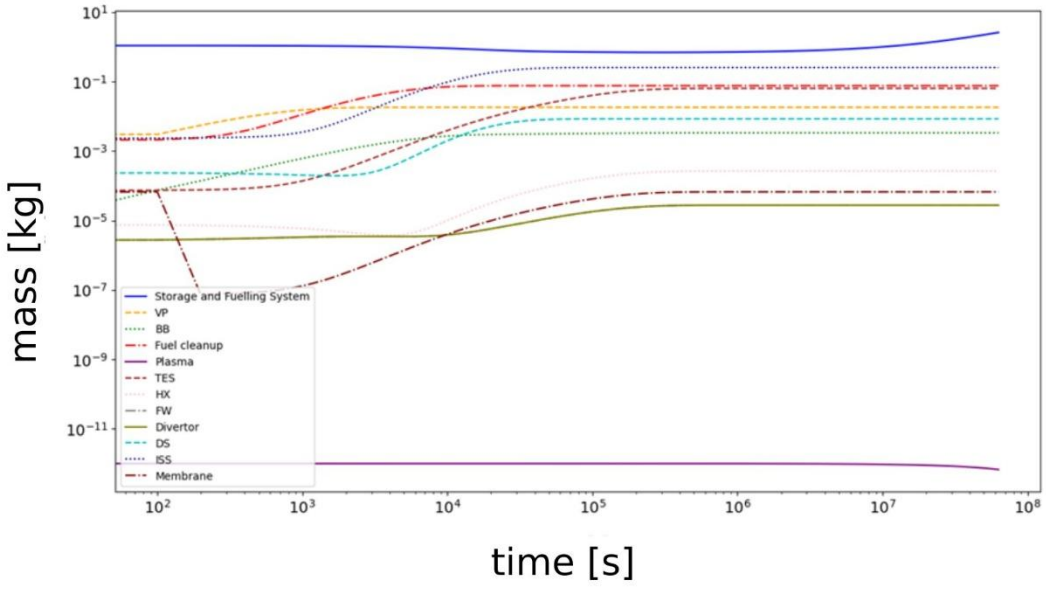

Figure 4 - Tritium inventories in the FC components with TBE = 0.02

1.4 Plasma operational regime

The plasma operational regime affects the continuity of pumping, tritium recovery, processing and reinjection dynamics.

The plasma can be operated in either steady-state or pulsed regime:

Steady State regime:

This configuration represents a useful approximation for time scales comparable to the tritium doubling time (on the order of several years). In this regime, the plasma is maintained continuously, typically through non-inductive current drive mechanisms such as lower hybrid waves or neutral beam injection. Steady-state operation simplifies inventory modelling and enables stable fuel injection and exhaust conditions.

Pulsed regime:

Expected to characterize the operation of the first generation of reactor-scale tokamaks (e.g., ITER, DEMO and ARC), the pulsed regime features discrete plasma discharges interleaved with dwell times. During dwell phases, the vacuum pumping system must re-establish ultra-high vacuum conditions, with pressures typically in the range of $10^{-6}\ Pa$. Although physically more representative of real machine behavior, this mode introduces strong time-dependent variations in tritium flows and inventories.

In this work, a continuous plasma approximation is adopted to simplify the numerical implementation and enable a tractable analysis of long-term tritium flows. Instead of explicitly modelling each individual pulse and the associated idle periods, a time-averaged approach is used. The Availability Factor (AF) accounts for the fraction of time during which the plasma is burning fuel. For pulsed regimes, an AF value of 0.7 is applied, reducing the injected fuel rate and so the fusion power by 30%, while preserving the total energy and tritium consumption over long timescales. This simplification enables the model to simulate the Fuel Cycle using a single continuous set of equations, while still capturing the average effect of pulsed operation.

Once the number of vacuum pumps required to sustain continuous plasma operation is determined under nominal steady-state conditions, the dwell phase requirements are verified. This step evaluates whether the same pumping system is also capable of restoring ultra-high vacuum conditions in the vacuum chamber during the dwell phase between two discharges. From this analysis, the minimum inter-pulse dwell time needed for full evacuation can be estimated, providing an important constraint for the reactor's operational scheduling and the design of the exhaust system.

1.5 Fuel composition

The isotopic composition of the fuel injected into the plasma significantly influences the fusion reaction rate, tritium consumption, and the dynamics of the exhaust and breeding systems. Two main configurations are typically considered in modelling: nominal (equal deuterium and tritium injection) and tritium-lean mixtures. These approaches differ not only in their impact on the Tritium Burning Efficiency (TBE), but also in how they affect pumping requirements and the overall isotope inventory.

Nominal plasma composition:

Same amount of tritium and deuterium are injected. It is the simplest approximation to be implemented.
Assumptions to be made are:

$$\dot{N}_D^{in} = \dot{N}_T^{in}$$

$$\theta_{DT} = \frac{D_D}{D_T} = 1$$

where $\dot{N}_x^{in}$is the injected flux of the isotope x and θ_{DT} is the ratio of diffusivity of the species [2]. The last hypothesis on deuterium and tritium diffusivity allows to obtain the same amount of deuterium and triutium in the divertor zone in this configuration. Later on, it will be discussed that an instantaneous transport to divertor zone is assumed for all the gas unburnt, generate or injected that must be pumped out.

Tritium-Lean Plasma:

In this scenario, a higher proportion of deuterium is injected relative to tritium, leading to an asymmetric fuel mixture. The primary motivation is to increase the TBE, as fewer tritium atoms are injected but a comparable fraction is still burned, thereby reducing the required tritium breeding rate and inventory. The details of this operating strategies are described in [2].

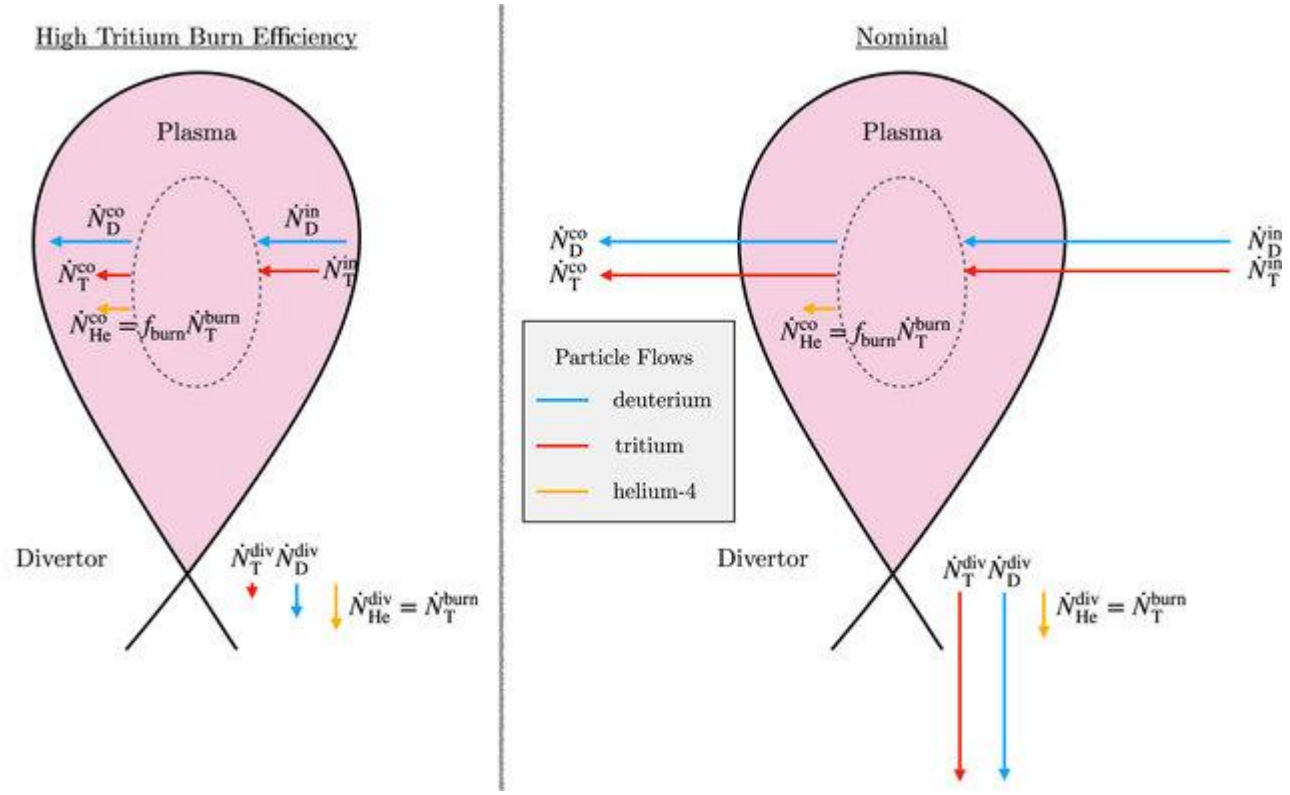

Figure 5 - Schematic of the particle flows in a tritium-lean and a nominal configuration, both at equal total fusion power. The arrows' magnitudes represent the size of the particle flows. In the tritium-lean case, the tritium flows are significantly smaller than the deuterium flows [2].

In addition to the core fuelling strategy, extra deuterium is often injected into the Scrape-Off Layer (SOL) to support and sustain H-mode confinement. Maintaining H-mode operation requires control over edge density and plasma-wall interactions, which can be regulated by gas puffing of deuterium near the divertor or midplane regions. Studies have shown that this additional deuterium can reduce edge-localized mode (ELM) amplitude and help maintaining favourable pedestal conditions, effectively increasing global confinement [3].

From a modelling perspective, this peripheral deuterium injection can be treated using a tritium-lean approximation even in cases where the core fuel composition is nominal (i.e., 50%-50%). In such cases, the *effective* tritium-to-deuterium ratio in the total injected flow—when

accounting for both core and edge fuelling—becomes skewed toward deuterium. This has implications for both the overall isotope inventory and the pumping system, as deuterium dominates the exhaust gas composition. The fuel cycle model can account for this by adjusting the input ratios accordingly, capturing the net transport and inventory effects of asymmetric fuelling strategies. Both approaches are considered from a modelling perspective in Section 3.3.

Chapter 2 – Vacuum Pumps technologies

Vacuum pumps play a critical role in fusion reactors, ensuring proper confinement and particle control by maintaining the required pressure conditions in the vacuum chamber.

Vacuum technologies are generally classified into three families:

- Positive displacement pumps
- Kinetic pumps
- Entrapment pumps

However, only a few technologies are compatible with the harsh conditions of a D-T fusion environment. For ITER and DEMO-class reactors (and in general, Fusion Power Plants FPPs), four major constraints must be addressed [4]:

1. High magnetic field tolerance
2. Resistance to gamma and neutron radiation
3. Safety against hydrogen explosions
4. Tritium compatibility and resistance to radioactive decay effects

Among the various available options, this study focuses on two pumping technologies that are both technically feasible and tritium-compatible:

- **Cryosorption pumps** (as developed and tested in ITER)
- **Vapor diffusion pumps**

These will be discussed in more detail in Sections 2.1 and 2.2, according to Figure 6.

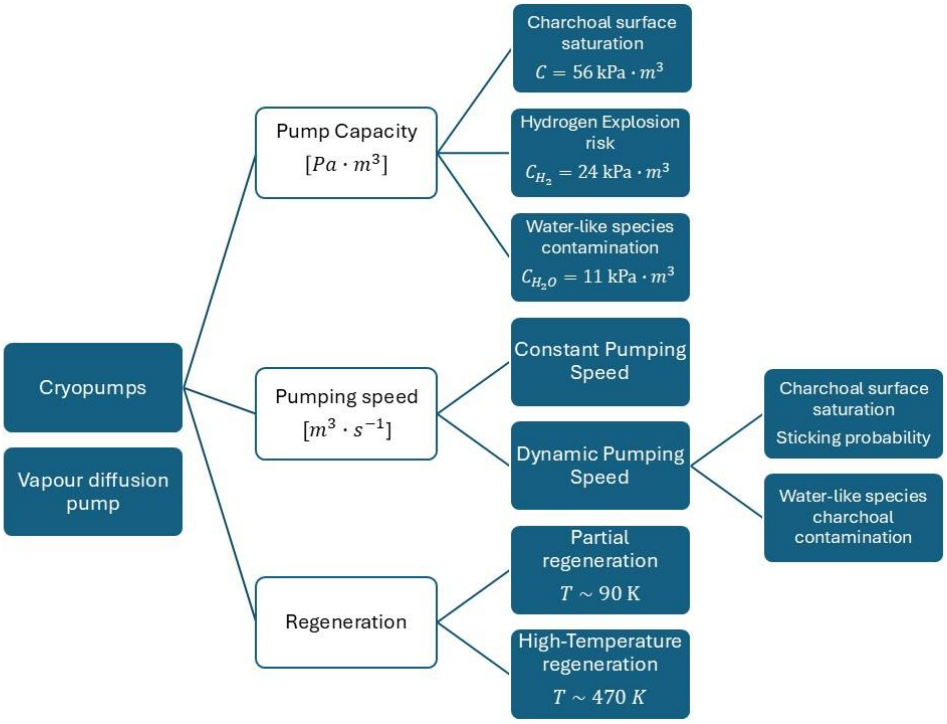

Figure 6 - Vacuum Pumping System complexity tree diagram adopted in this work

Their operation is essential in two distinct regimes:

- During plasma operation, when exhaust gases are continuously extracted from the divertor region to be recycled or processed.
- Between plasma discharges, especially in pulsed machines, when pumps must restore ultra-high vacuum conditions in the main chamber. This is necessary to ensure reproducible and clean plasma initiation in the next pulse.

In this work, a continuous plasma approximation is used for modelling purposes. As previously described, the Availability Factor (AF) accounts for the duty cycle of plasma operation. After the number of pumps required for steady-state operation is determined, a post-processing verification is performed to ensure that the same pumping configuration can restore vacuum conditions between pulses. This makes it possible to estimate the minimum dwell time between discharges.

In Sections 2.1.1, 2.1.2, 2.1.3, 2.1.4, focus is on the main physical mechanisms governing vacuum pump operation: capacity, pumping speed, valve, and regeneration.

The view of ITER pumping system is shown in Figure 7.

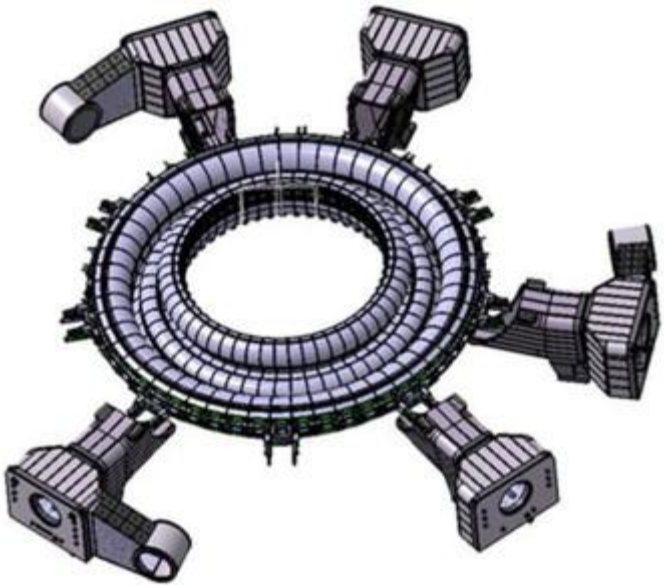

Figure 7 - View of ITER vacuum pumping system with 5 direct and 3 branch ducts [5].

2.1 ITER cryosorption pump

In this section the working principle of a cryopump is described, taking ITER cryosorption pump as reference.

A cryopump is an entrapment vacuum pump that removes gas molecules by capturing them on cryogenically cooled surfaces rather than expelling them like mechanical pumps. It operates through two main mechanisms: cryocondensation, where gases cool below their saturation pressure and condense into a solid phase, and cryosorption, where non-condensable gases like helium and hydrogen are adsorbed onto porous materials such as charcoal or zeolites. The required temperatures for condensation vary depending on the gas, as shown in Figure 8. with ~100 K sufficient for water and hydrocarbons, ~20 K for nitrogen and oxygen, and ~4 K for hydrogen isotopes and neon.

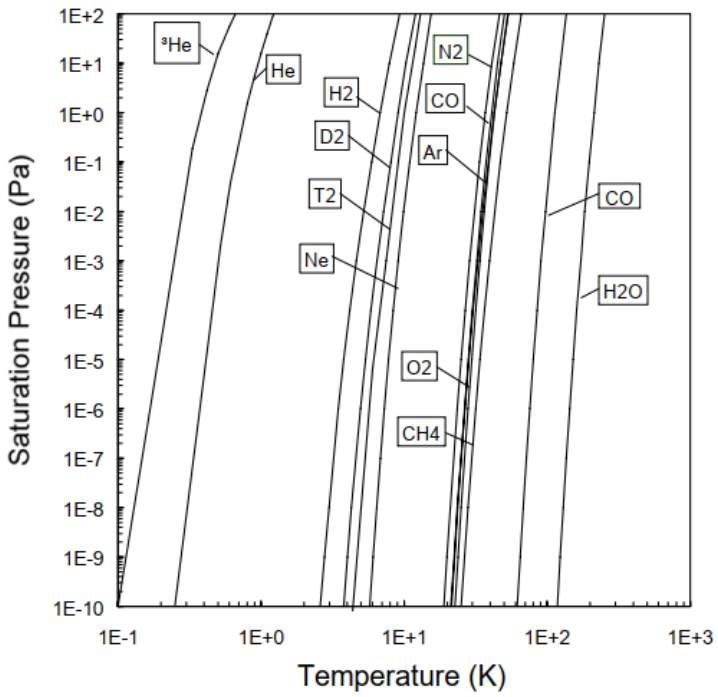

Figure 8 - Saturation curves of common gases [6].

Unlike cryocondensation, which relies on the phase change of gases into liquids or solids upon cooling, cryosorption involves the physical adhesion of gas molecules onto the large internal surface area of a sorbent material. The most commonly used sorbent in cryopumps is activated charcoal. This material is highly porous, offering a vast internal surface area which makes it particularly effective for adsorbing light gases otherwise difficult to condense. When the charcoal is cooled to cryogenic temperatures, the kinetic energy of gas molecules becomes low enough for van der Waals forces to dominate, allowing molecules to adhere to the surface of the pores. This process is reversible, meaning the adsorbed gases can be desorbed by warming up the material.

The geometry and mesh of the ITER divertor and pumping duct is shown in Figure 9.

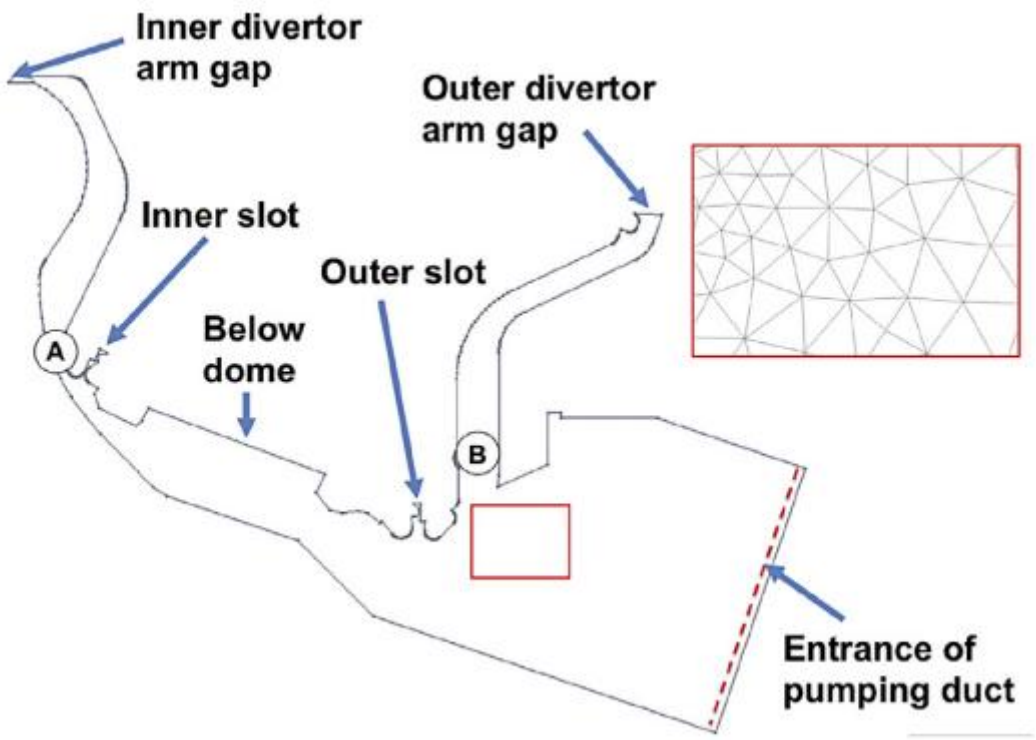

Figure 9 - ITER sub-divertor geometry [7].

Cryopumps are crucial in nuclear fusion due to their high pumping speed and ability to process large gas flows, making them ideal for deuterium-tritium fuel cycles in devices like JET and ITER. They are typically cooled using liquid helium (4–5 K) from the reactor's cryoplant and are designed to be tritium-compatible. However, their pumping capacity is finite, as gas accumulation eventually saturates the surfaces, reducing efficiency. When full, they must undergo regeneration, where they are warmed to release trapped gases before resuming operation. The regeneration phase enforces a batch-mode operation, which raises scalability challenges for FPPs. So, precise modelling is essential to evaluate its integration into a full-scale fuel cycle.

The main parameters to characterize a cryopump, shown in Figure 10, are pump capacity, pumping speed, valve and regeneration strategy.

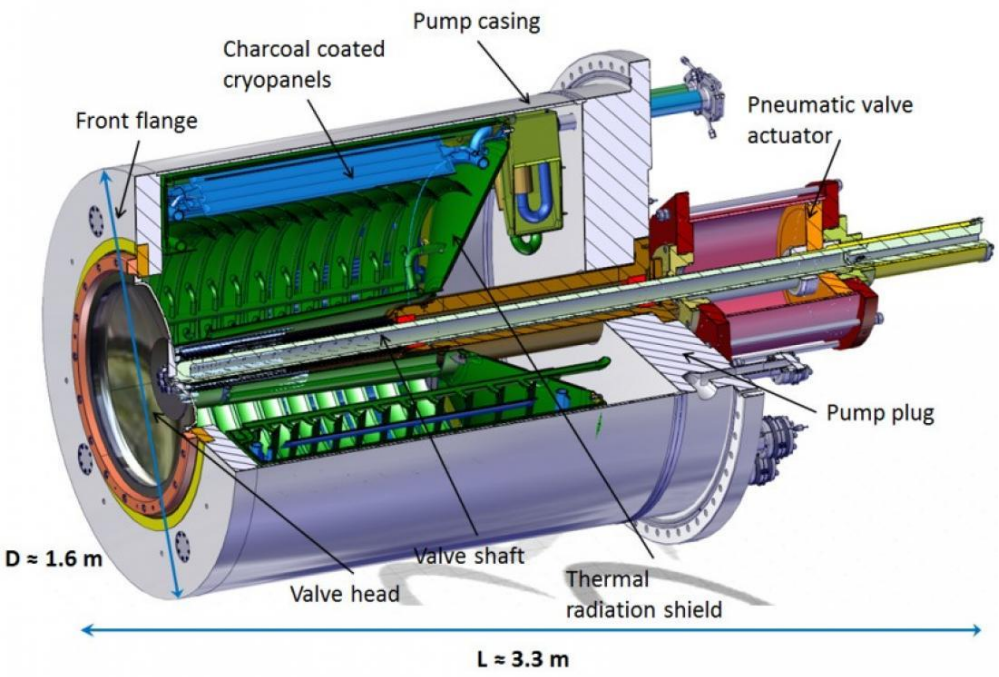

Figure 10 - ITER torus cryopump [5].

2.1.1 Pump capacity

The maximum capacity of a cryogenic pump is a critical design parameter, especially in fusion environments where large quantities of hydrogen isotopes must be handled safely and efficiently. In this work, two main criteria are used to define the capacity limit of an ITER-class cryosorption pump:

1. Saturation of the adsorbing surface
2. Hydrogen explosion risk threshold
3. Water-like species saturation limit

Saturation Limit

The first limiting factor arises from the finite adsorption capacity of the cryogenic surfaces. The ITER cryopump is equipped with 28 hydroformed panels coated with charcoal (Figure 11), with an effective adsorbing area of approximately $A_{ads} = 11.2\mathrm{m}^2$ [8] and the maximum gas load per unit area is typically taken as [2]:

$$L_{max} = 0.5Pa\frac{\mathrm{m}^3}{\mathrm{cm}^2} = 5\ \mathrm{kPa}\frac{\mathrm{m}^3}{\mathrm{m}^2}$$

Therefore, the maximum pumping capacity due to surface saturation is:

$$C_{sat} = A_{ads} \cdot L_{max} = 56\ \mathrm{kPa} \cdot \mathrm{m}^3$$

This value represents the total volume of gas that can be retained before the surface becomes fully saturated and requires regeneration.

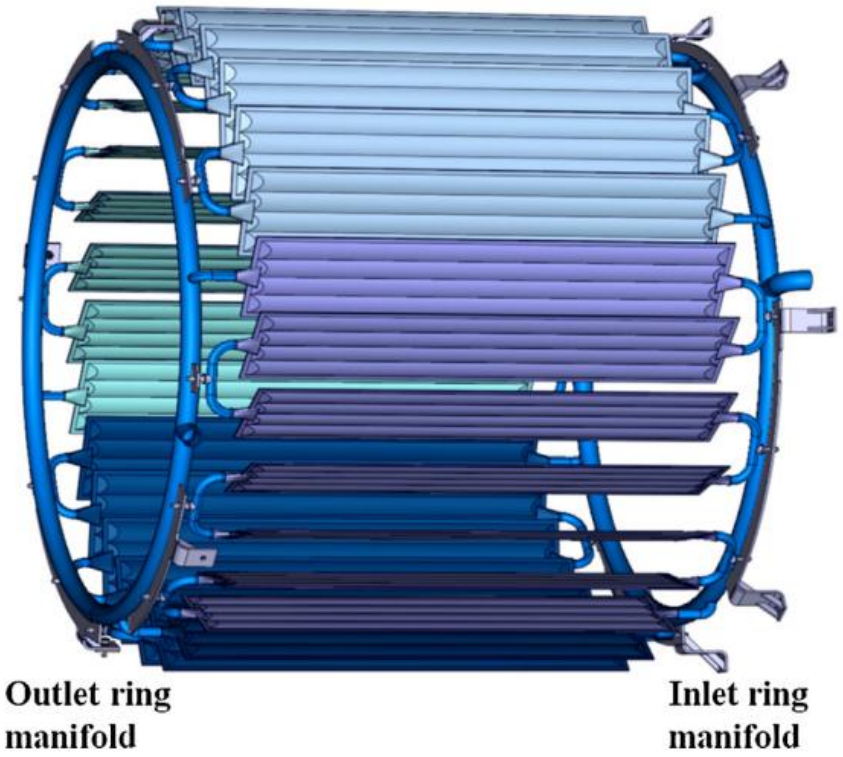

*Figure 11 - The cryopanels of the ITER cryopump made of 28 similar hydroformed panels. All panels will be coated with charcoal on both sides. Each has 1*m *x 0.2*m *size for a total charcoal surface of 11.2*m^2 [8].

Explosion Risk Limit

The second capacity constraint comes from hydrogen safety considerations. Accumulation of hydrogen isotopes in the pump volume must not exceed concentrations that could lead to flammable or explosive conditions. We assume a maximum allowable partial pressure of hydrogen (in $1\mathrm{m}^3$) of [2]:

$$P_{expH_2} = 1.7\mathrm{kPa}$$

Which is well below the lower flammability limit ($\sim 4\%$ volume or 4kPa in $1\mathrm{m}^3$) and a pump internal volume of:

$$V_{pump} = 14\ \mathrm{m}^3$$

This was increased in the ITER project from $8\mathrm{m}^3$ when the number of pumps was decreased from 8 to 6 in the design of the vacuum pumping system [5].

The explosion-limit-based capacity is:

$$C_{\exp_{H_2}} = P_{expH_2} \cdot V_{pump} = 23.8\ \mathrm{kPa} \cdot \mathrm{m}^3$$

This value must be strictly respected in any operating condition, as exceeding it would pose severe safety risks. It is important to note that this threshold applies only to hydrogenic species (H_2, D_2, T_2), and should not account for helium or injected impurities such as PEGs (plasma enhancement gases), which do not contribute to flammability.

Water-like species limit

It is necessary to limit the accumulated tritium inventory in the form of tritiated impurities, such as water or higher hydrocarbons. A conservative assumption is made on the maximum water load on the charcoal surface of:

$$L_{H_2O,max} = 0.1\ \text{Pa} \cdot \frac{\text{m}^3}{\text{cm}^2}$$

Resulting in a max water-species capacity of:

$$C_{H_2O} = A_{ads} \cdot L_{H_2O,max} = 11.2\ \text{kPa} \cdot \text{m}^3$$

Discussion on high-temperature regeneration are made in the regeneration chapter.

For reference, a comparison can be made with commercially available cryopumps. The KDCP-50SHIN-IC-S model (Figure 12) from CryoPride™ [9] lists a maximum hydrogen capacity of 150 standard liters (sL). Converting this to the units used above:

$$150\text{sL} = 150 \cdot 10^{-3}\text{m}^3 \cdot 101325\ \text{Pa} = 15.2\ \text{kPa} \cdot \text{m}^3$$

This value is of the same order of magnitude as the ITER pump capacities calculated above, confirming that the adopted estimates are realistic and aligned with industrial standards.

Figure 12 - KDCP-50SHIN-IC-S model from CryoPride™ [9] has a $15.2\ kPa \cdot m^3$ *capacity for hydrogen.*

2.1.2 Pumping speed

The pumping speed S of a vacuum pump quantifies the volumetric flow rate at which it can remove gas from the vacuum vessel. The throughput Q of the pump is the product of its pumping speed and inlet pressure p.

$$Q = p \cdot S$$

Throughput is typically measured in units of Pa·m^3/s, which represents the volumetric flow rate (in m^3/s) multiplied by the gas pressure (in Pa). These units are particularly useful in the

molecular flow regime, where the relationship between pressure and flow becomes non-linear and depends on the molecular behaviour of the gas.

Depending on the plasma conditions and local geometry, the Knudsen number (Kn)—defined as the ratio of the molecular mean free path to a characteristic system length—can vary significantly throughout the divertor region of a fusion reactor. In the upper divertor and near the targets, the gas typically operates in the slip flow regime ($10^{-3} \leq Kn < 0.1$), whereas in the sub-divertor region and inside the vacuum pumps, the gas enters the transitional ($0.1 \leq Kn < 10$) or even the free molecular regime ($Kn \gg 1$), where inter-molecular collisions are rare and surface interactions dominate [10]. In these latter regimes, gas behaviour is best described by kinetic theory, and parameters such as pumping speed and molecular throughput ($Pa \cdot m^3/s$) become more physically meaningful than bulk pressure gradients.

In the molecular regime, the pumping process involves individual gas molecules impinging on a cold surface and either condensing or being adsorbed, making parameters like sticking probability and transmission probability critical to determining the actual gas removal rate. These effects are captured quantitatively by the capture coefficient, discussed in detail below.

As a first approximation, pumping speed can be considered constant during steady-state operation. However, as saturation of the adsorbing surface progresses, variations in pumping speed are expected. These effects are addressed in the next subsection. Furthermore, results from Monte Carlo (MC) simulations [11] are introduced to justify the final modelling choice adopted in the fuel cycle code.

2.1.2.1 Capture coefficients

The pumping speed for a gas species can be expressed as:

$$S = c\, S_{id} = c\, A_{inlet} \sqrt{\frac{R_0 T}{2\pi M}}$$

where:

- S is the effective pumping speed;
- c is the capture coefficient, accounting for geometrical and gas-surface interaction losses;
- S_{id} is the ideal pumping speed, based on kinetic theory of gases;
- $A_{inlet}$is the inlet area of the pump;
- $R_0$is the universal gas constant;
- T is the temperature;
- M is the molar mass of the gas.

The capture coefficient depends on two main factors: the transmission probability through baffles or geometrical constraints, and the sticking probability of the gas on the cryogenic surface. The relationship is:

$$\frac{1}{c} = \frac{1}{\alpha} + \frac{1}{w} - 1$$

where:

- α is the sticking probability, i.e. the fraction of molecules that stick upon first impact;
- w is the transmission probability, i.e. the fraction of molecules that reach the adsorbing surface.

Values for α and w are listed in the table below and are based on a parametric characterization that has been performed for the ITER type charcoal under ITER-relevant conditions and on characteristic parameters for a standard refrigerator cryopump. [6]

Table 2 - Capture coefficients for a standard cryopump

Gas	w	α	c
T_2	0.4	1	0.40
D_2	0.4	0.9	0.38
He	0.25	0.25	0.14

For Plasma Enhancement Gases (PEGs), an assumption of c = 0.4 is reasonable, due to expected condensation at 5 K.

However, it is important to note that in the present model, the values of w and α have not been explicitly used to compute the pumping speed. Instead, a different modelling strategy has been adopted, relying on Monte Carlo simulations. These simulations directly provide the effective pumping speed, incorporating the effects of gas-surface interactions and internal reflections without needing to separately estimate α, w, or c. The results and implications of this approach will be discussed in detail in the following sections.

2.1.2.2 Monte Carlo simulation for unloaded-surface pumping speed

To characterize the intrinsic performance of cryopumps, Luo et al. conducted Monte Carlo simulations to model the transport and capture of gas particles in complex vacuum systems. These simulations allow the prediction of the effective pumping speed by tracking the trajectories of individual gas molecules within the cryopump geometry and calculating their probability of being captured on the cold surfaces [11].

Results from MC simulations revealed that the effective pumping speed is almost insensitive to the type of gas being pumped, despite significant differences in their sticking coefficients. For example, helium and deuterium, which exhibit very different sticking probabilities ($\alpha_{He} \approx 0.2$ vs. $\alpha_{D_2} \approx 0.9$), were shown to produce comparable effective pumping speeds in Figure 13 and Figure 14.

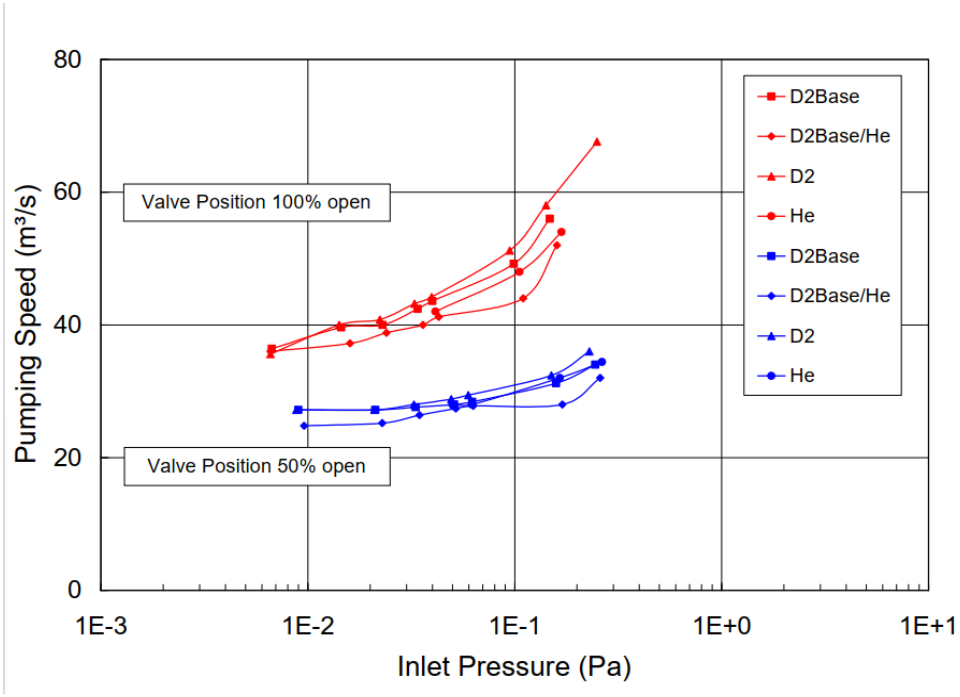

Figure 13 – Monte Carlo simulations show similar pumping speed for Helium and Deuterium despite very different sticking probability.

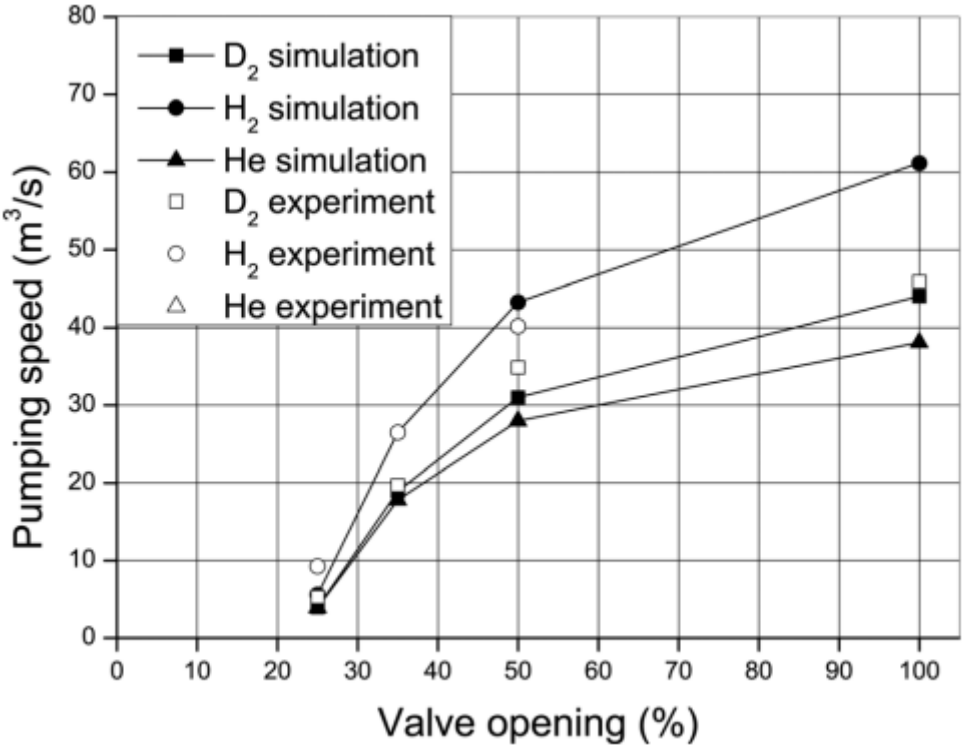

Figure 14 – Experiment and simulation show similar pumping speed for Helium and Deuterium despite very different sticking probability [11].

This counterintuitive result can be explained by considering the multiple interaction opportunities that a gas molecule experiences within the cryopump. Even if the sticking coefficient is relatively low, such as in the case of helium, the complex internal geometry forces particles to undergo numerous reflections before exiting. This increases the cumulative

probability of capture. As a consequence, once the sticking coefficient is above a certain threshold (typically $\alpha \geq 0.1$), the molecule is likely to be adsorbed after a limited number of bounces, making the pumping speed relatively independent of the exact value of α (Figure 15).

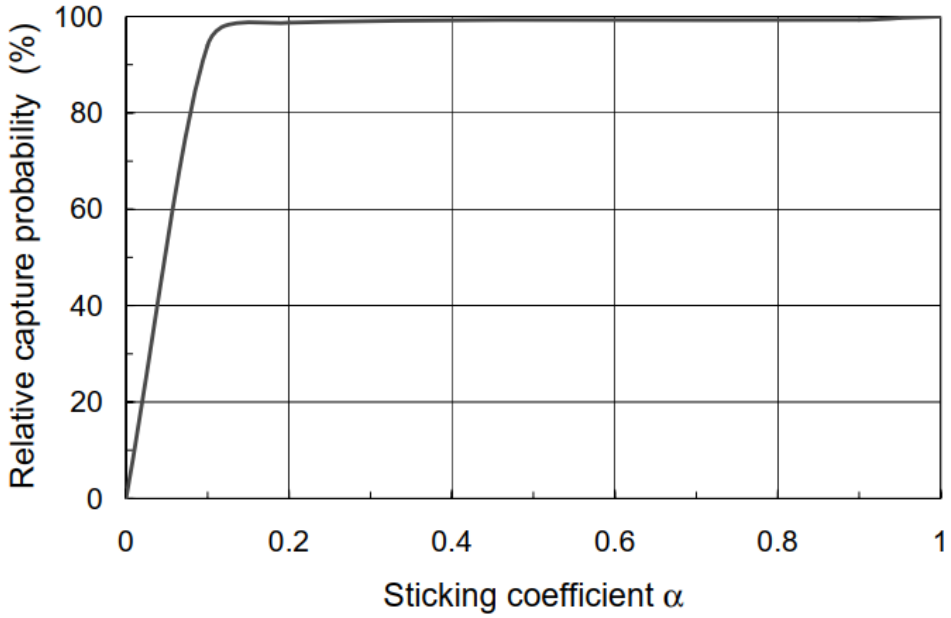

Figure 15 - Relative capture probability against sticking coefficient in an ideal cryopump [6].

These simulation results will be used in the present fuel cycle model to represent the initial pumping speed of a fresh, unloaded cryosorption surface. This constitutes the reference condition at the beginning of operation. In the following section, we will address how this initial performance degrades over time as the surface becomes progressively saturated with adsorbed gas, leading to a reduction in the effective pumping speed.

2.1.2.3 Dynamic pumping speed

The pumping speed of cryosorption pumps is not constant over time, but decreases progressively as the charcoal surface becomes saturated, as visible in Figure 16. This reduction is due to the decreasing availability of free condensation and adsorption sites for incoming particles [5].

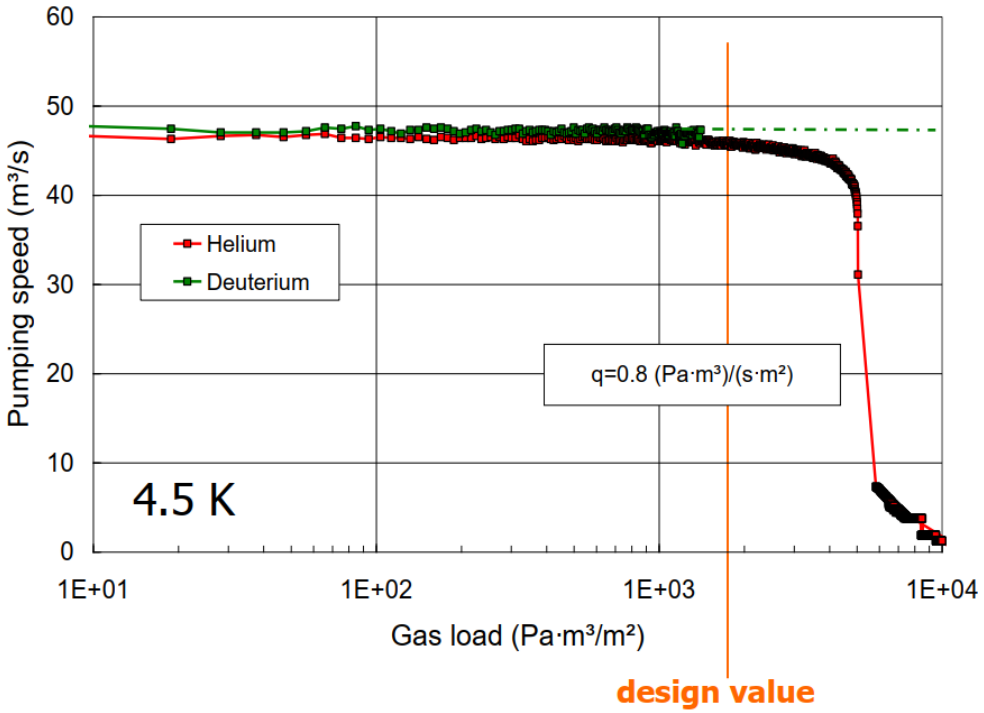

Figure 16 - Helium shows huge degradation of pumping speed beyond ITER designed point [12].

The pumping speeds calculated in the previous section—under the assumption of an unloaded surface—are used here as initial values, corresponding to the beginning of operation when the surface is completely clean. To describe the evolution of the pumping speed as a function of surface saturation, an empirical sigmoid correlation has been adopted.

The dynamic pumping speed for each gas species is defined by the following relation:

$$S_x(\gamma) = S_{x\_0} \cdot \left(1 - \frac{\gamma^4}{\gamma^4 + (1-\gamma)^4}\right)(1-\gamma)^{1-\alpha}$$

where:

- S_{x_0} is the initial pumping speed of species *x*, corresponding to an unloaded surface
- γ is the surface saturation, defined as the ratio between inventory and capacity:

$$\gamma = \frac{I_{pump}}{C_{pump}}$$

- α is the sticking probability of the species

This formulation captures two essential behaviours: a smooth and progressive reduction of pumping speed as the surface fills, and a species-dependent degradation rate modulated by the sticking coefficient. In particular, gases with higher sticking coefficients tend to maintain effective pumping performance longer, whereas species with lower α values experience a more rapid decline.

It is important to note, however, that in typical operating conditions, cryopumps are used within a controlled range of saturation, well below full capacity, to ensure safety against hydrogen explosion hazard. As a result, the actual reduction in pumping speed over time is often modest and not significantly detrimental to system operation.

Moreover, pumping speed is going to decrease with the amount of water-like substances that contaminates the surfaces. However, this effect shows a reduction of 10%, according to Figure 17 [13].

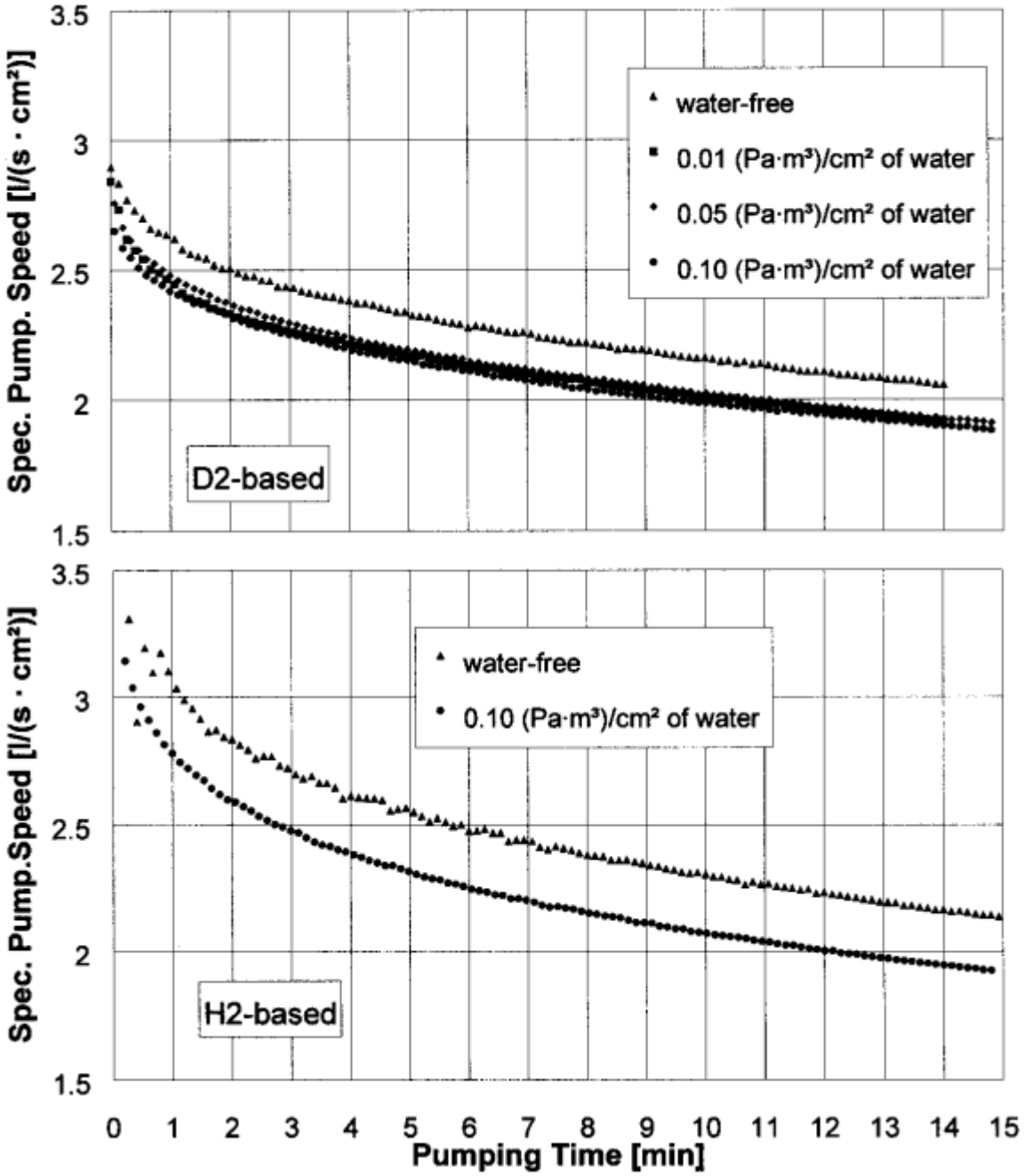

Figure 17 - Pumping speed results (related to the cryosorption panel surface) as a function of pumping time at maximum throughput conditions and various water preloadings [13].

2.1.2.4 Model assumptions for pumping speed

In the design of ITER's cryogenic pumping system, the optimal pumping speed has been identified in the range of 60–80 m^3/s per pump, based on a trade-off between throughput requirements and vacuum system conductance limitations (Figure 18). Higher pumping speeds are generally desirable to ensure rapid removal of hydrogen isotopes and helium from the divertor region. However, increasing the nominal speed beyond a certain threshold offers diminishing returns due to conductance constraints imposed by the ducts and valve geometry, which limit the effective speed as seen from the divertor plenum. Additionally, larger pumping capacities would require more frequent regeneration or increased physical dimensions, affecting integration and maintenance feasibility.

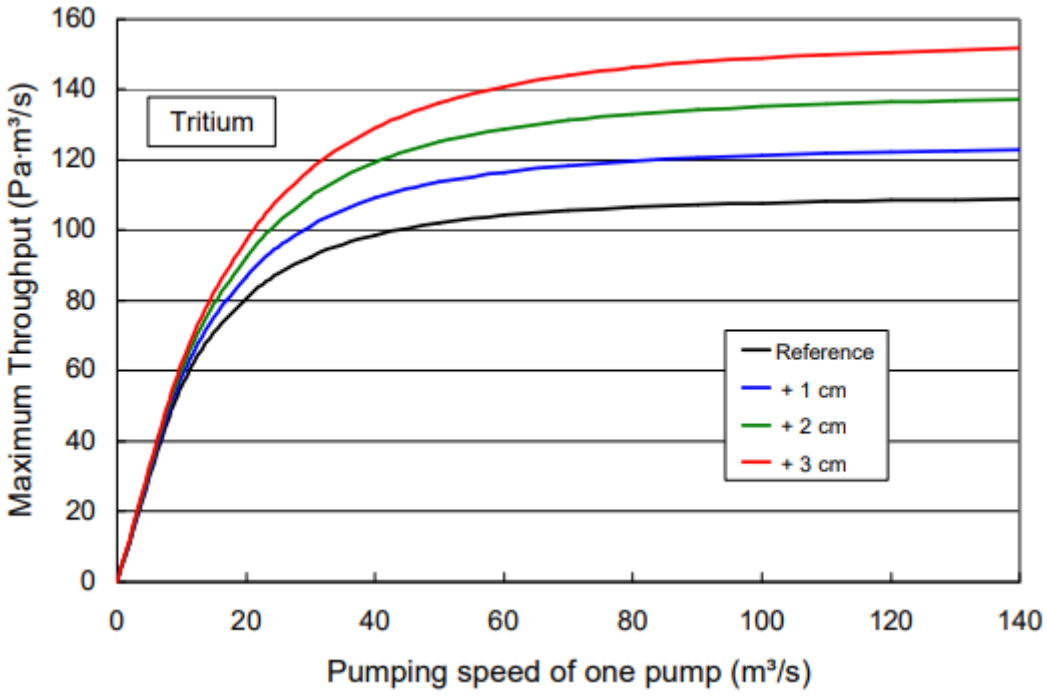

Figure 18 -Maximum achievable ITER throughput for a divertor pressure of 2 Pa for the heaviest hydrogen isotope T_2. The curves highlight the impact of increased cross-sections at each of the three divertor fingers per duct (by 1/2/3 cm in both directions) [14].

In the present model, a dynamic pumping speed is adopted to reflect the real performance degradation over time due to surface saturation, as described in the previous section and shown in Figure 19. The initial pumping speed, corresponding to the unloaded (clean) surface condition, is determined based on the results from Monte Carlo simulations.

The initial values differ among gas species due to their molecular mass, which influences the molecular velocity distribution and, consequently, the capture probability at the pump surface. Further discussion on the Section 3.2.1.

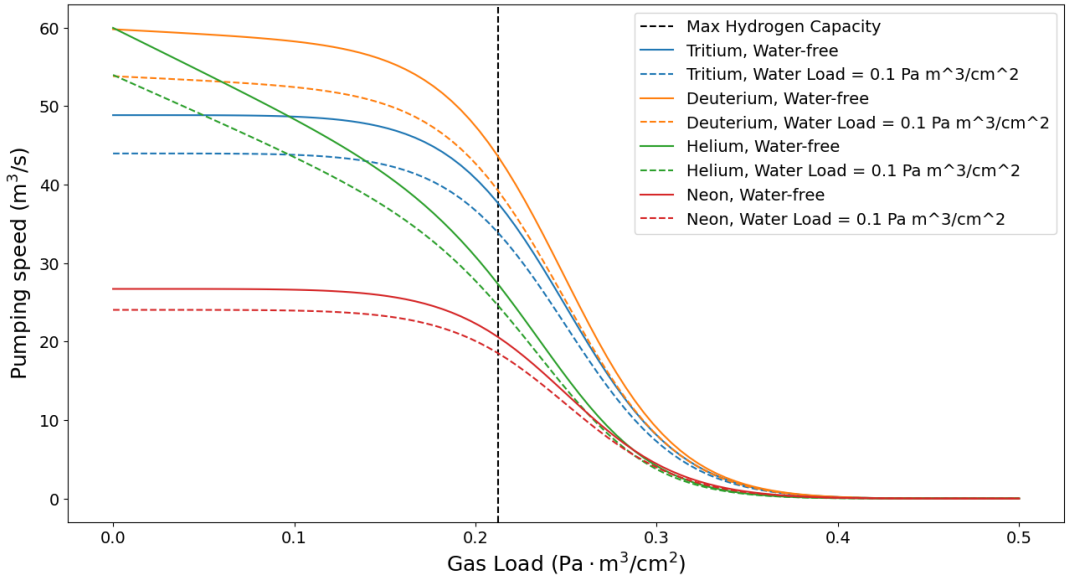

Figure 19- Dynamic Pumping Speed adopted in the model.

2.1.3 Valve

Each cryopump is equipped with an inlet valve (Figure 20), which plays a critical role in controlling the total gas throughput entering the pump. This valve acts as a physical constraint, ensuring that the incoming gas flow remains within operational and safety limits, such as the maximum allowable hydrogen inventory (to prevent potentially explosive concentrations) and the total adsorption capacity of the pump.

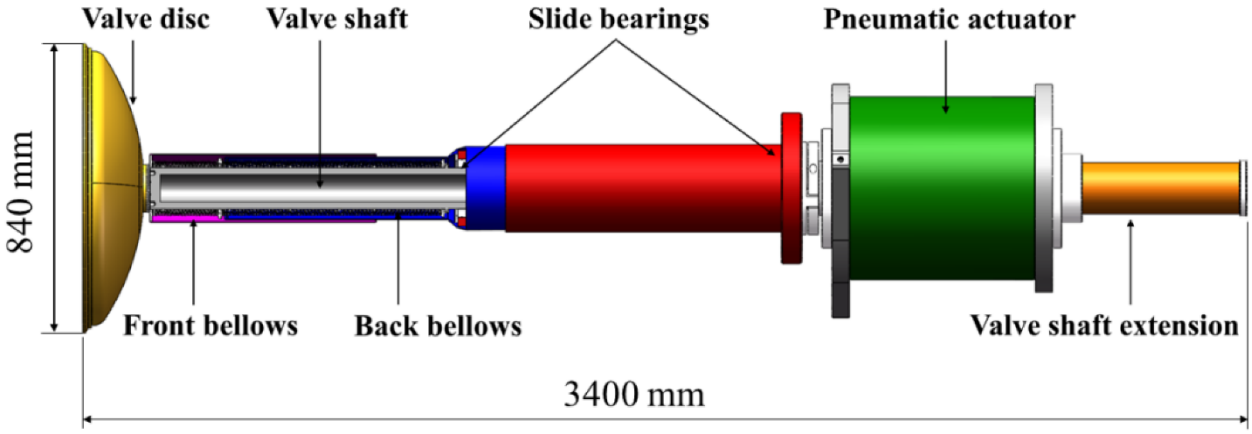

Figure 20 - Overview structure of the inlet valve of a CFTER torus cryopump [15].

In the model, two different valve management strategies have been implemented, depending on the operating assumptions of the vacuum system:

- **Single-valve approach**: A single valve regulates the total flow of the gas mixture entering the pump. This approach is used when the pressure at the pump inlet is imposed as a fixed boundary condition. It reflects the behavior of a real cryopump,

where a single physical valve throttles the entire mixture, limiting the overall mass flow rate to prevent exceeding capacity or safety thresholds.

- **Multi-valve approach (n valves)**: When the pressure at the pump inlet is solved iteratively—as part of the overall system dynamics—each gas species is assigned its own virtual valve (with n= number of species). This numerical strategy allows:
    - individual control of the throughput per species, ensuring that none of the partial flows exceeds the physical or numerical constraints,
    - avoiding unphysical negative densities in upstream volumes,
    - and capturing the pressure evolution of each species in the divertor region due to accumulation and differential pumping behavior.

Although this method does not reflect the hardware configuration of an actual cryopump, it is essential for the numerical stability and accuracy of the model. This multi-valve formulation enables the system to account for species-dependent effects and pressure buildup, which are critical in the dynamic simulation of the fuel cycle.

The implications of these two approaches, and their influence on the physical interpretation of the model, will be discussed in more detail in Section 3.4 Divertor density and pressure.

2.1.4 Regeneration

Under regeneration, the cryopump is warmed up, the gas released and pumped out via the forepumping system, and finally cooled again.

The temperature of regeneration must be chosen as low as possible to reduce cryogenic needs for re-cooling of the pumping panels.

Three steps of regeneration are proposed:

- partial regeneration at 90-100K
- second step at ambient temperature to the release of all air-like species
- high temperature at 470K to release water-like substances

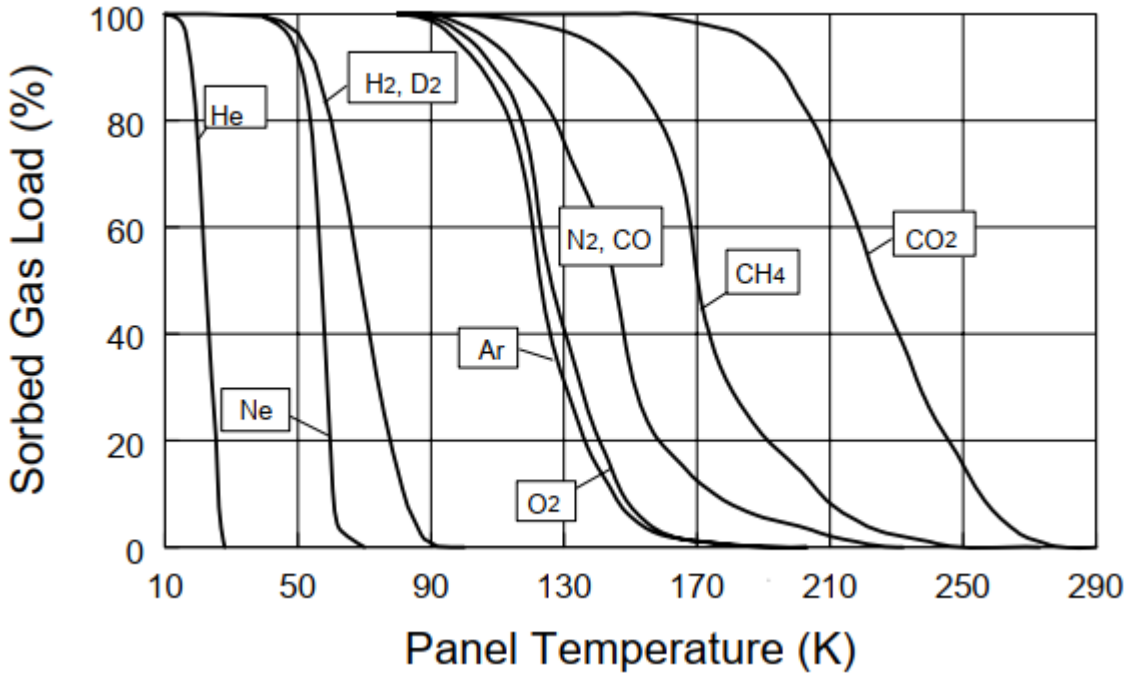

Figure 21 - Temperature-induced desorption curves [16] .

2.1.4.1 Partial regeneration

In pumping operation the cryopanels are cooled by supercritical helium at 0.4 MPa and an inlet temperature of about 4.4K.

The partial regeneration step is performed at a charcoal temperature of 90–100 K to release all hydrogen isotopes (and helium), as shown in Figure 22.

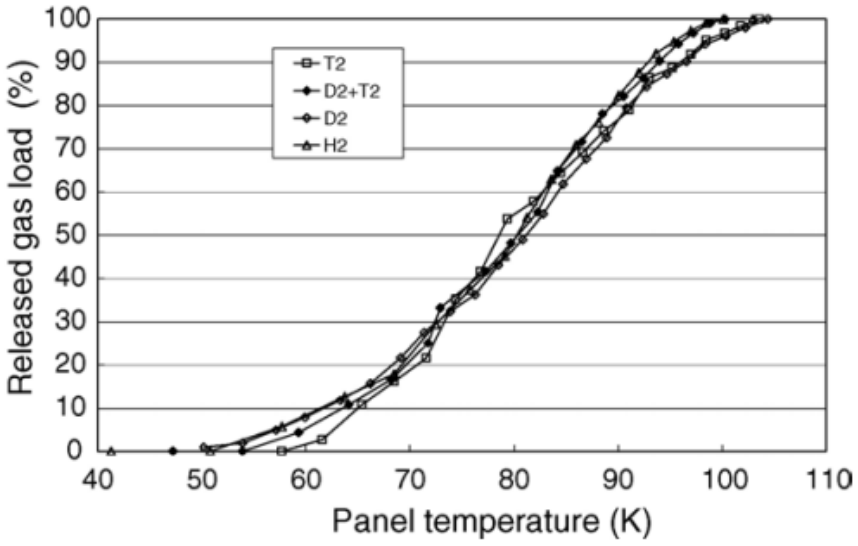

Figure 22 - Hydrogen release curves for the different hydrogen isotopes during regeneration [17].

2.4.1.2 High-Temperature regeneration

The second step at ambient temperature leads to the release of all air-like species, but not water-like species [18]. In this step the cryopanels are regenerated to 300K using helium at 1.8 MPa.

Any water-like species with strong sorption bonding forces need still higher temperatures for effective desorption from the charcoal, as shown in Figure 23.

Considering the set-up of the real ITER cryopump, all water-like substances will at first be condensed at the inlet baffle system (at 80 K) and, from that respect, will not immediately interact with the sorption panels. However, within high temperature regeneration, the condensed species will evaporate as soon as the temperature becomes equivalent to the boiling temperature at the corresponding partial pressure. The water-like molecules, then in gaseous phase, will instantaneously be sorbed by the charcoal, as the sorption capacity is still relatively high at this temperature level. By that mechanism, the inventory of all gas species, no matter where pumped at first, will be defined by sorption/desorption processes.

These species in their tritiated forms may contribute significantly to the semi-permanent tritium inventory; a good knowledge of their regeneration characteristics is therefore essential for tritium inventory control.

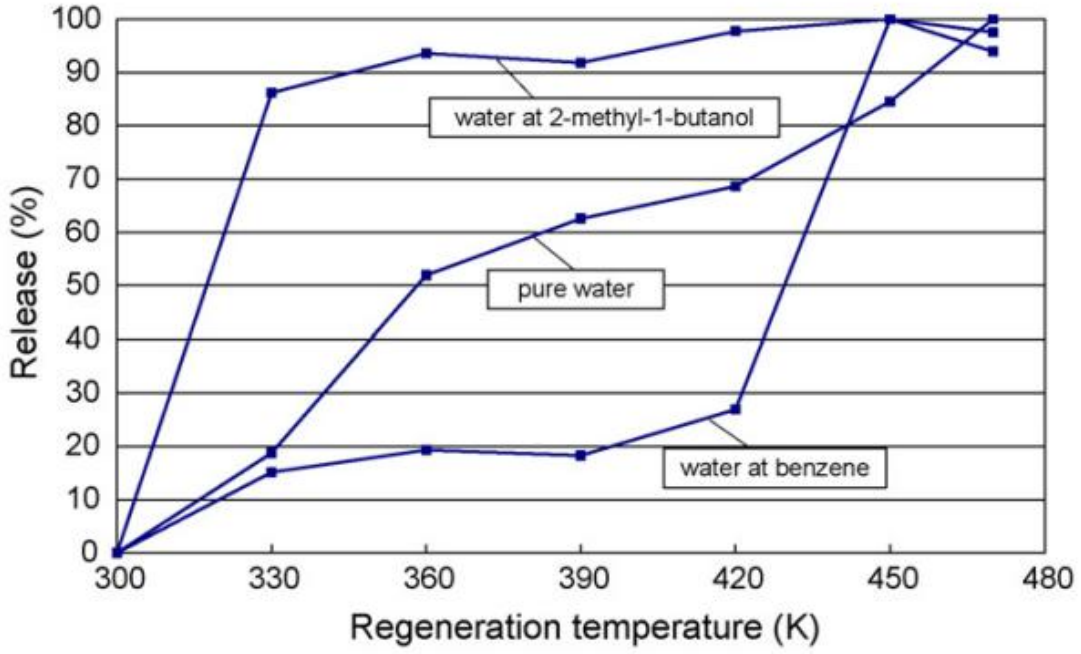

Figure 23 - Regeneration curves for pure water and in combination with hydrocarbons [18].

For the release of water and decontamination of the cryopump the cryopanels can also be heated to 470K. For the high temperature regeneration helium at 1.2 MPa will be used.

The 470 K level puts additional requirements on the cryopump system design. First, the warm gas at 470 K will supply the cryopump in the same piping which normally carries cryogenic gaseous helium. This adds special requirements to instrumentation, valves, etc. and leads to cost increase. Secondly, the pressure drops in the cryopanel and shield circuits of the cryopumps are high under high temperature conditions. Thirdly, at 470 K tritium permeation

through the walls of the cryogenic piping into the helium circuit of the cryoplant is starting to develop. This may play a role if extensive operation at 470 K will become a need.

Desorption from a sorbent can also be stimulated by pressure reduction. However, this is a much slower process and is therefore only used to increase sorption efficiency in parallel to the usual temperature increase.

The water gas load of interest in this investigation is defined by the order of magnitude typical for ITER. The plasma exhaust gas has a specified maximum water content of 0.5% [13].

2.1.4.3 Regeneration Strategy

In the context of a fusion reactor fuel cycle, cryopump regeneration is a necessary process to prevent overaccumulation of hydrogen isotopes and preserve safe and effective pumping performance. While ITER adopts a staggered operational strategy—with pumps alternately taken offline for regeneration to ensure continuous vacuum operation (Figure 24)—in this model, that approach is not implemented. Instead, the regeneration logic is based on inventory thresholds and hierarchical pump management.

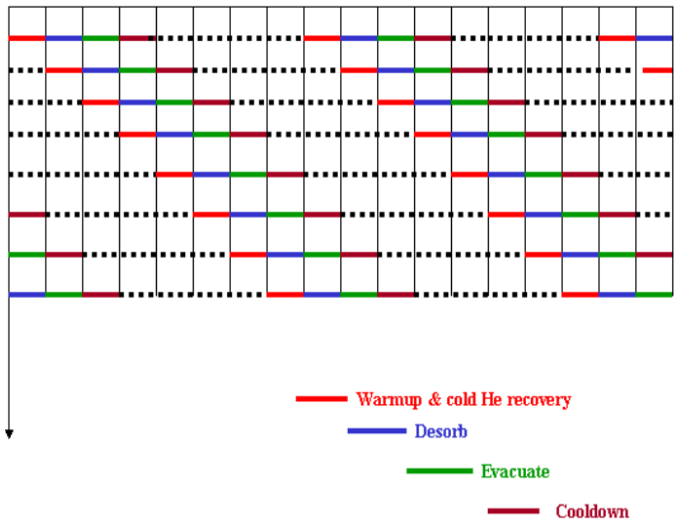

Figure 24 - ITER staggered operation regime [12]

A cryopump is assumed to undergo a partial regeneration cycle when one of the following conditions is met:

- The hydrogen inventory reaches the maximum allowed threshold, which is defined by safety constraints (e.g., explosion risk). Since hydrogen isotopes are the dominant species in a D–T fusion environment, this is typically the primary trigger for regeneration.
- The total gas inventory (including helium and impurities) reaches the maximum capacity of the pump. However, in a D–T environment, this scenario is less likely due to the relatively low accumulation rate of non-hydrogen species.

- The pump is temporarily inactive due to a stand-by state in the hierarchical control logic. This occurs when a previously inactive upstream pump is reactivated, making the downstream pump redundant for a time. If the inactive pump still contains a non-negligible inventory, it may be regenerated in advance during its stand-by phase to restore full capacity in anticipation of future reactivation.

The regeneration process duration is derived from ITER data and assumed to be a fixed downtime per pump (typically 600s), during which the cryosorption surface is warmed up, outgassed, and evacuated before returning to operational temperature. This duration is implemented as a constant in the model and is applied whenever a regeneration event is triggered.

Furthermore, a full high-temperature regeneration cycle is triggered when the accumulated amount of water-like species in the cryopump reaches its maximum allowed capacity. Although air-like species are not explicitly tracked in the gas mixture within the simulation code, this high-temperature cycle also serves to desorb and remove such residual gases from the surfaces. The duration of the full regeneration is fixed at 6000 seconds, which is ten times longer than that of a partial regeneration cycle.

2.2 Vapour diffusion pump

In fusion reactor vacuum systems, vapour diffusion pumps are investigated as a potential alternative to conventional cryogenic pumping systems, especially within the framework of continuous-operation fuel cycle concepts. A notable example is the KALPUREX process [19], which combines vapour diffusion pumps with liquid ring pumps to continuously extract exhaust gases from the divertor region without requiring periodic regeneration phases.

The working principle of vapour diffusion pumps relies on a high-speed jet of vapour (such as oil or mercury) injected through a nozzle system into a vertically mounted chamber (Figure 25). Gas molecules entering the pump are entrained by the vapour stream and driven toward the pump base, where they are removed by a backing pump. The process involves no moving mechanical parts.

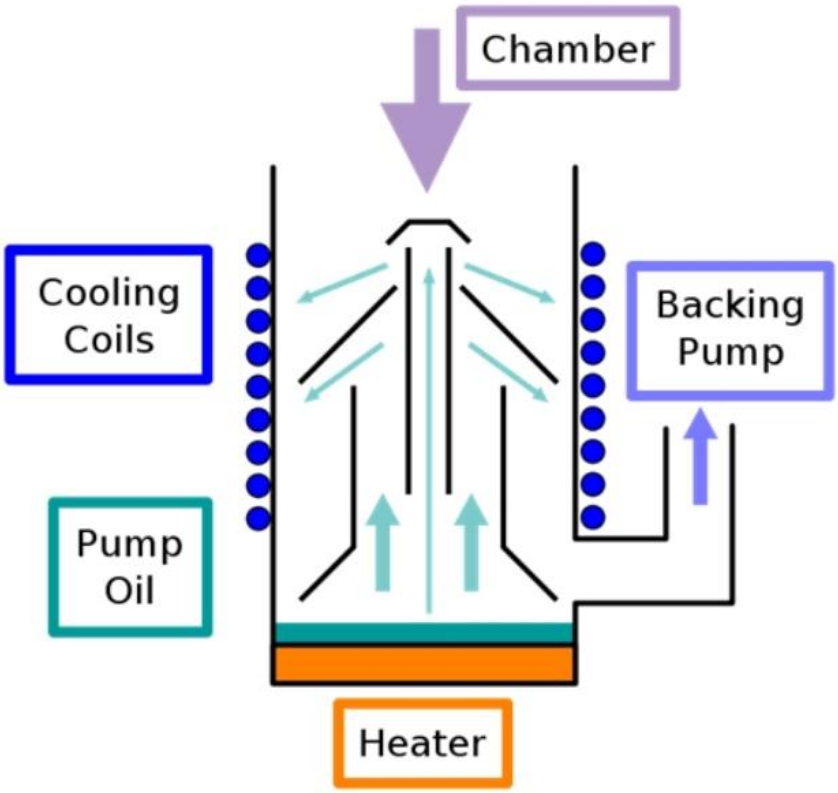

Figure 25 - Schematic illustration of a diffusion ejector pump [20].

Vapour diffusion pumps meet three main requirements in a D-T fusion reactor:

- High pumping speed – The vapour jet entrains a significant volume of gas, allowing the system to sustain high throughput, which is crucial given the high exhaust rates from the plasma.
- Tritium compatibility – In KALPUREX [19], mercury is applied due to its tritium compatibility. It must be made sure that the working fluid stays inside the pump and that any mercury vapour propagation in the system is effectively avoided
- Continuous operation – The vapour diffusion pump operates in a steady state, allowing for uninterrupted exhaust gas handling and significantly simplifying the system compared to cryopumps, which require periodic warm-up and re-cooling phases.

In the model, continuous operation represents a huge simplification of the system, since it doesn't require any regeneration strategy to be applied.

Chapter 3 describes the physical model of a cryosorption pump, which can be adapted to vapour diffusion pump with straightforward simplifications.

Chapter 3 - Physics modelling

3.1 Equation of state

In the divertor region of a nuclear fusion power plant, the gas pressure is sufficiently low to justify the use of the ideal gas law as an accurate approximation for the thermodynamic behavior of the system.

$pV = vRT = Nk_BT$ or $p = nk_BT$

where v is the number of moles, R is the universal gas constant ($8.314\ J \cdot mol^{-1}K^{-1}$), k_B is the Boltzmann constant ($1.3805 \cdot 10^{-23} J \cdot K^{-1}$), N is the number of particles and n is the number density of particles.

In this work, the microscopic form of the ideal gas law $p = nk_BT$ is primarily used, as it provides a direct link between the macroscopic pressure and the particle density in each control volume. This formulation is particularly suitable for particle-based modeling of the fuel cycle, where species are tracked individually and the pressure must be updated based on local accumulation rates.

The validity of the ideal gas assumption holds due to the relatively low densities and high temperatures present in the divertor, where gas–gas and gas–wall interactions can be neglected in first-order approximation.

3.2 Chemical species

This work considers five gaseous species in the divertor and vacuum system: deuterium (D_2), tritium (T_2), helium (He), neon (Ne), and water-like substances. Each plays a specific role in the plasma environment and directly impacts the performance and saturation behavior of the cryopumping system.

Deuterium is one of the two fusion fuels and is typically injected in large excess compared to tritium. A tritium-lean fuel mixture is preferred to reduce the radiological hazard and simplify handling. As a result, deuterium is usually the most abundant hydrogenic species in the exhaust, significantly contributing to the cryopump load and to the hydrogen inventory constraints.

Tritium, the radioactive component of the fuel, is injected in smaller quantities but is central to fusion power production. Its accumulation in the vacuum system must be strictly monitored due to safety concerns, including the hydrogen explosion risk, which considers the combined inventory of all hydrogen isotopes in the cryopump.

Helium is the main fusion product from deuterium-tritium reactions. It is chemically inert and does not participate in further reactions, but its accumulation in the plasma leads to dilution, reducing fusion performance if not efficiently exhausted. From a vacuum technology

perspective, helium is particularly challenging: due to its extremely low boiling point, cryocondensation is not effective under the typical operating conditions of fusion cryopumps. Therefore, cryosorption is employed instead, where helium is captured via physic adsorption onto porous materials such as activated charcoal cooled to very low temperatures. This mechanism is less efficient than condensation pumping and strongly depends on surface saturation, making helium one of the limiting factors for long-term cryopump performance. Helium particles flow to the pump simulation is shown in Figure 26.

Neon is injected as Plasma Enhancement Gases (PEGs) to promote radiative cooling and facilitate plasma detachment in the divertor region. Though introduced in smaller quantities, this noble gas can accumulate and contribute to the total gas load on the cryopump. Typically, PEGs represent 4–5% of the total divertor gas composition [21].

Water-like substances have only been considered for their non-negligible impact on charcoal surface poisoning and the resulting regeneration requirements. Their partial pressures and specific pumping speeds are not explicitly characterized in the model, as they constitute only a minor fraction (approximately 0.5%) of the total plasma exhaust.

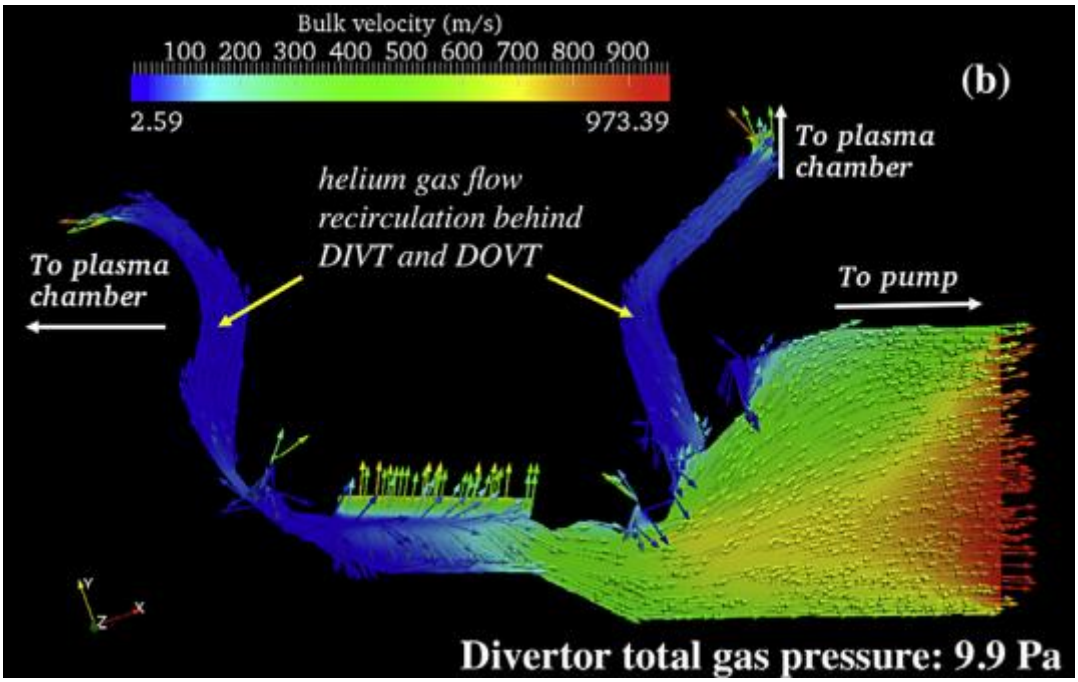

Figure 26 - Helium particles flow towards the plasma chamber through DIVT and DOVT for the case where the total divertor pressure is 9.9 Pa [7].

3.2.1 Pumping speed ratio for different species

The fundamental quantity describing the gas-handling capability of a vacuum pump is the throughput, which represents the amount of gas removed per unit time. In its basic form, throughput is defined by the relation:

$$Q = pS$$

In the context of a fusion reactor, the vacuum system must handle a mixture of gases, each with different physical and chemical properties. Therefore, the total throughput of a cryopump is the sum of the partial throughputs of each gas species:

$$Q_{pump} = \sum_x Q_x = \sum_x p_x^{div} S_x$$

where:

- Q_{pump} is the total throughput [Pa·m^3/s],
- Q_x is the partial throughput of species x,
- p_x^{div} is the partial pressure of species x in the divertor dome region [Pa],
- S_x is the pumping speed for species x [m^3/s].

Pumping speed depends on both the gas and the pump's geometry and surface properties. From kinetic theory, it is known that lighter molecules move faster on average and thus reach the pump surface more frequently. Consequently, pumps tend to handle lighter gases more efficiently, assuming all other conditions are equal.

The ideal pumping speed of a species can be expressed as:

$$S^{id} = A_{inlet} \sqrt{\frac{R_0 T}{2\pi M}}$$

Given this dependence on molar mass, the ratio of ideal pumping speeds for two species (assumed to be at the same temperature) can be expressed as:

$$\frac{S_{x1}^{id}}{S_{x2}^{id}} = \sqrt{\frac{MM_{x2}}{MM_{x1}}}$$

In the present model, the pumping speed for deuterium was used as the reference value, since it has been previously determined through a combination of experimental measurements and Monte Carlo simulations of the cryopump geometry and internal gas dynamics.

The pumping speeds for all other species were then derived analytically from this reference using the ideal gas scaling law based on molar mass:

$$S_x^{id} = S_{D_2}^{id} \sqrt{\frac{MM_{D_2}}{MM_x}}$$

As previously discussed, the effective pumping speed for each species depends not only on molecular mass but also on the capture coefficient, which reflects the probability that a molecule hitting the cryopump surface will be retained. This relationship is expressed as:

$$S_x = c_x^{capt} S_x^{id}$$

However, in this work, the available pumping speed data already incorporate the effect of capture coefficients. That is, the reported values represent the effective pumping speeds, not the ideal ones.

Therefore, to estimate the pumping speeds for other species in the model, we directly apply the molar mass scaling law starting from the effective pumping speed of deuterium

$$S_x = S_{D_2}\sqrt{\frac{MM_{D_2}}{MM_x}}$$

This approach ensures consistency with simulation data while allowing for a simplified yet physically meaningful representation of the species-dependent pumping behavior.

3.3 Divertor flow rates

Unburnt fuel (deuterium and tritium), helium ash, and plasma enhancement gases are continuously exhausted from the plasma core and must be removed through the vacuum pumping system located in the divertor region.

The flow rates of fuel and helium at the divertor are directly linked to the fuel injection rate and the burning efficiency of the plasma. In a D-T fusion reaction:

$$D + T \rightarrow He + n$$

one helium nucleus (alpha particle) is produced for each pair of deuterium and tritium nuclei consumed. Thus, the helium production rate is equal to the number of tritium nuclei burned per second. Defining $\dot{N}_{T_{burn}}$ as the tritium burn rate:

$$\dot{N}_{He_{prod}} = \dot{N}_{T_{burn}}$$

A key performance indicator for plasma operation is the Tritium Burning Efficiency (TBE), which quantifies the fraction of injected tritium that is actually consumed in fusion reactions. It is defined as:

$$\mathrm{TBE} = \frac{\dot{N}_{T_{burn}}}{\dot{N}_{T_{in}}} = \frac{\dot{N}_{T_{burn}}}{\dot{N}_{T_{burn}} + \dot{N}_{T_{div}}}$$

For a given reactor thermal power—and thus a fixed tritium burn rate —the amount of fuel that must be exhausted by the vacuum pumping system is strongly dependent on the Tritium Burning Efficiency. The flow rate of unburnt tritium reaching the divertor can be expressed as:

$$\dot{N}_{T_{div}} = \dot{N}_{T_{burn}}\left(\frac{1-\mathrm{TBE}}{\mathrm{TBE}}\right)$$

A more refined expression accounts for a small fraction of tritium that is not exhausted—being instead retained by plasma-facing components such as the first wall and the divertor:

$$\dot{N}_{T_{div}} = \dot{N}_{T_{burn}}\left(\frac{1-\mathrm{TBE}-f_{FW}-f_{div}}{\mathrm{TBE}}\right)$$

where:

- f_{FW} is the fraction of tritium impinging onto the first wall,
- f_{div} is the fraction impinging onto the divertor structure.

The deuterium exhaust flow rate can be described analogously:

$$\dot{N}_{D_{div}} = \dot{N}_{T_{burn}} \left(\frac{k_{DTin} - \mathrm{TBE}}{\mathrm{TBE}} \right)$$

Where:

- $k_{DTin} = \frac{\dot{N}_{D_{in}}}{\dot{N}_{T_{in}}}$

Here, the coefficient k_{DTin} accounts for deviations from a perfectly balanced fuel composition:

- $k_{DTin} = 1$ corresponds to the ideal case of a 1:1 D:T ratio
- $k_{DTin} > 1$ reflects tritium-lean fuelling strategies or additional deuterium introduced

On the other hand, the helium exhaust flow rate depends solely on the thermal power of the reactor, as helium is produced directly by the fusion reactions:

$$\dot{N}_{He_{div}} = \dot{N}_{T_{prod}} = \dot{N}_{T_{burn}}$$

This relation explicitly highlights a key assumption adopted in the model: instantaneous transport from the plasma core to the pumping system. While this simplification neglects detailed transport delays and redistribution effects, it maintains the balance between model simplicity and physical relevance.

As for Neon, the exhaust rate corresponds to the amount injected during steady-state operation. Neon is used to manage radiative cooling at the divertor but must be carefully regulated to avoid excessive fuel dilution. In the model, its total contribution to the gas load is estimated by:

$$\dot{N}_{Ne_{div}} = 0.04 \, (\dot{N}_{T_{div}} + \dot{N}_{D_{div}} + \dot{N}_{He_{div}})$$

This assumption reflects typical PEG concentrations (4–5%) observed in the divertor region under advanced plasma scenarios [22].

These equations define the set of fixed particle flow rates that must be exhausted by the vacuum pumping system. In Section 3.4, a discussion on the divertor region's pressure and particle densities will provide the necessary framework to link these flow rates to the total throughput of the pumping system.

3.4 Divertor density and pressure

From the vacuum pumping (VP) system's perspective, the divertor particle flow rate for a given species *x* is determined by the neutral gas density n_x^{div} and the effective pumping speed S_x^{VP}, according to the relation:

$$\dot{N}_{x_{div}} = n_{x_{div}} S_{x,VP}$$

Here, $S_{x,VP}$ represents the total active pumping speed of the VP system for species x, and it is calculated as the sum of the contributions from all the active pumps:

$$S_{x,VP} = \sum_{j=1}^{n_{pumps}} S_{x,j} \varphi_j$$

Where:

- $S_{x,j}$ is the pumping speed of the pump j for the specie x
- $\varphi_j \in [0,1]$ is the valve opening coefficient of the pump j

In this framework, $S_{x,VP}$ is treated as an unknown to be determined. One of the key objectives of the model is to identify the minimum number of cryopumps required for continuous operation. Consequently, the simulation must dynamically determine the number of active pumps at any given time based on the required total throughput.

To compute the effective pumping speed, and thus the number of active pumps, it is necessary to determine the inlet gas density or pressure in the divertor region. Two different approaches are implemented in the model:

Physics-Based Analytical Method: This approach uses known particle flow rates, the surface area of the divertor, and the ion acoustic speed to estimate the neutral pressure. It results in a set of fixed partial pressures for each species.

Iterative Numerical Method: This alternative approach models gas accumulation in the divertor region over time, adjusting the pressure and density iteratively to reflect dynamic operating conditions.

Both methods will be discussed in detail in the Sections 3.4.1 and 3.4.2.

3.4.1 Physics-based analytical method for density and pressure

When analysing gas density and pressure in the divertor region, it is essential to distinguish between different characteristic zones (Figure 27):

- The midplane edge plasma density $n_{x_{MP}}$,
- The recycling region density at the divertor targets $n_{x_{rec}}$,
- The pumping zone density $n_{x_{div}}$, which is the relevant quantity for evaluating vacuum pumping performance.

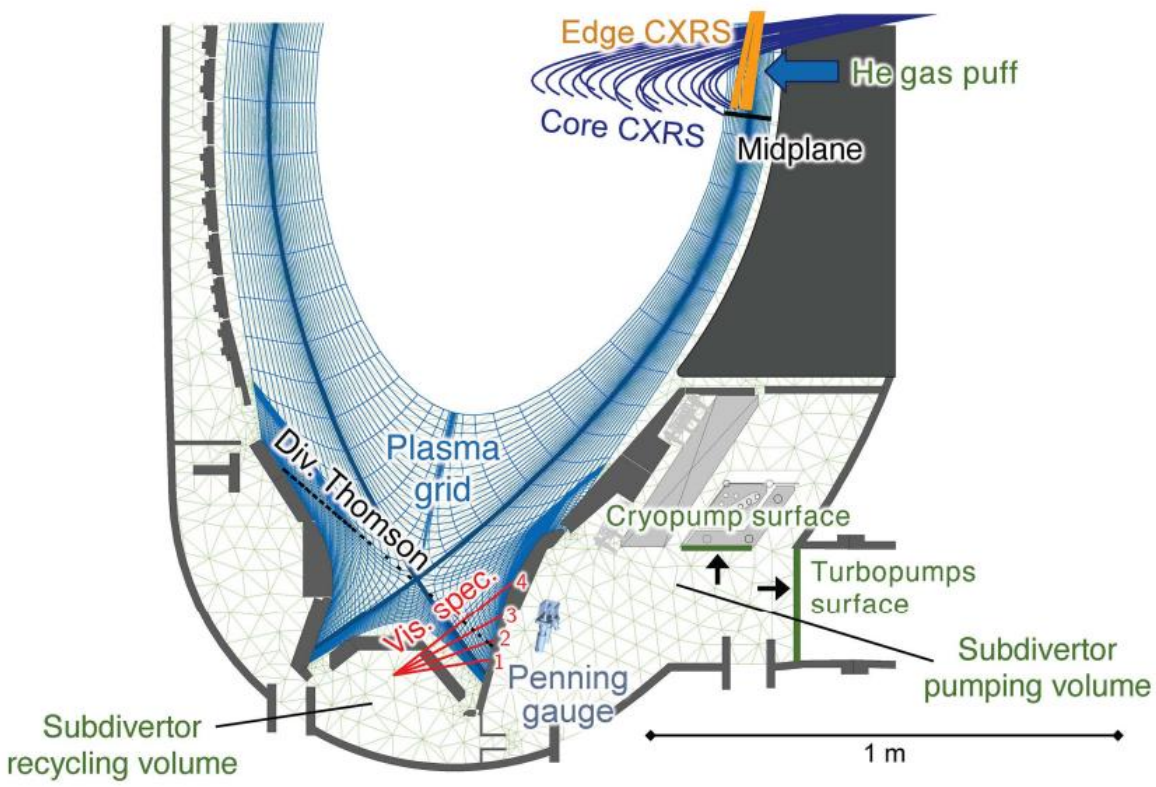

Figure 27 - ASDEX experiment in which He has been injected to study it's divertor dynamic. Adapted from [23].

Two key variables are:

$$C_x = \frac{n_{x_{rec}}}{n_{x_{MP}}}; R_x = \frac{n_{x_{rec}}}{n_{x_{div}}}$$

where:

- C_x is the **divertor compression**, the ratio between density in the subdivertor recycling volume and ion density in the edge at the plasma midplane. It describes the interplay between transport and recycling.
- R_x is the **sub-divertor density ratio**, the ratio between subdivertor neutral densities in the recycling and pumping volumes. It quantifies the efficiency with which atoms are transported towards the pumping volume, from which they can be finally permanently removed from the vessel.

Both C_x and R_x depend on detailed plasma transport physics and divertor geometry. While a full treatment is beyond the scope of this work, literature and experimental data (particularly for helium) suggest that the density at the pumping port is typically greater than at the target by a factor of about 4, as shown in Figure 28. Therefore, in this model, we adopt the following simplification for all species:

$$\frac{n_{x_{VP}}}{n_{x_{target}}} = 4 \; \forall x$$

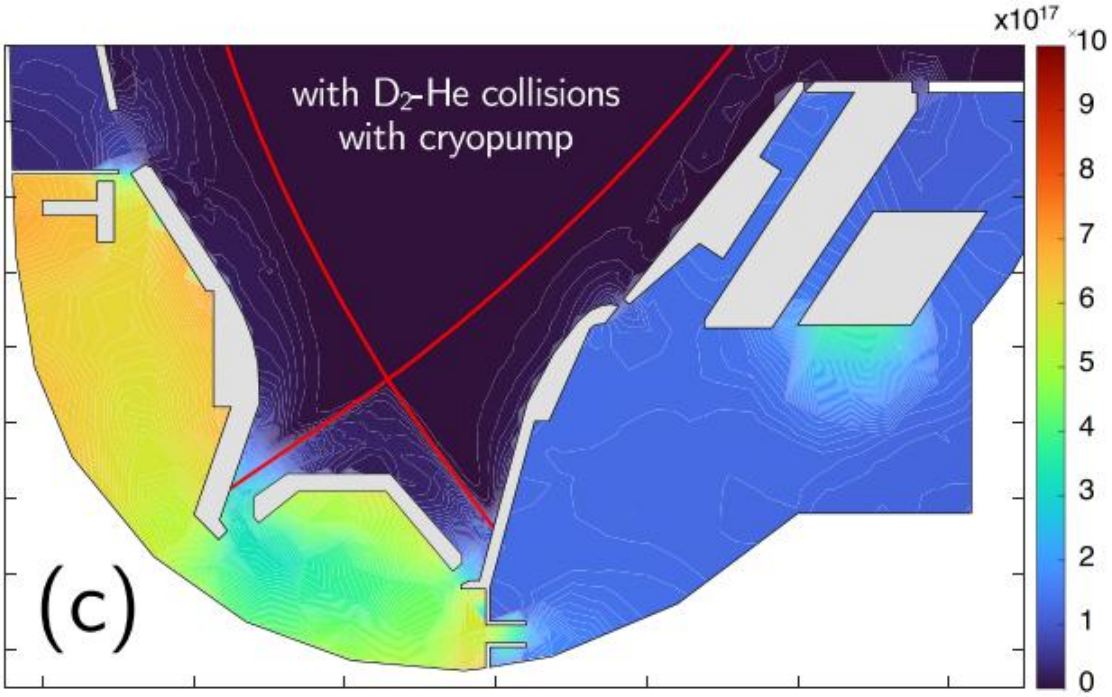

Figure 28 - Distribution of the simulated neutral He atom density in the entire subdivertor region for activated D2-He elastic collisions and cryopump effective for He atoms, i.e. imposing the same capture coefficient as for D2 molecules. [23]

From this point onward, all calculations will use the target density $n_{x_{target}}$. Whenever the pumping-zone density $n_{x_{VP}}$ is required, it will be obtained simply as

$$n_{x_{VP}} = 4n_{x_{target}}$$

A simple approximation of target density of the species x is the following:

$$n_{x_{target}} = \frac{\Gamma_x}{c_x} [\mathrm{m}^{-3}]$$

where:

- Γ_x is the particle flux in the divertor zone
- $c_x$is the ion acoustic speed of the species x

The particle flux Γ_x can be estimated from the ratio between the particle flow rate and the effective area of the divertor receiving the flux:

$$\Gamma_x = \frac{\dot{N}_{x_{div}}}{A_{div}} [\mathrm{m}^{-2}\mathrm{s}^{-1}]$$

Here, $\dot{N}_{x_{div}}$ is the particle flow rate of species *x*, and A_{div} is the divertor surface area being hit by the plasma exhaust. The latter can be estimated based on the power balance in the scrape-off layer (SOL):

$$A_{div} = \frac{\Phi_{SOL}}{q''_{max}} [\mathrm{m}^2]$$

where:

- Φ_{SOL} is the minimum power expected to be exhausted through the SOL (expected for ITER reactor $\sim 100\text{MW}$)
- q''_{max} is the maximum tolerable heat load on the divertor surface, determined by material limits (e.g., for tungsten, typically assumed as $10\ \text{MWm}^{-2}$)

resulting on

$$A_{div} \sim 10\text{m}^2$$

The ion acoustic speed c_x depends on the electron temperature at the divertor and is inversely proportional to the square root of the ion mass. It is defined as:

$$c_x = \sqrt{\frac{k_B T_e}{m_x}} [\text{ms}^{-1}]$$

where:

- T_e is the electron temperature at the divertor, typically around $T_e \sim 1\text{eV}$
- m_x is the ion mass of the specie x

For typical values of T_e and considering the lightest species (hydrogen isotopes), the ion acoustic speed is on the order of:

$$c_x \sim 10^4\ \text{ms}^{-1}$$

More results and discussion will be provided in Section 4.3.1 Physics-based analytic method.

3.4.2 Iterative numerical method for density and pressure

As previously stated, we assume instantaneous transport of neutral gas into the divertor region. The iterative numerical method models the accumulation of non-pumped gas over time. At each time step, any species that is not fully pumped out will begin to accumulate in the divertor, causing a local increase in its partial pressure. This, in turn, increases its throughput in the next time step, eventually reaching a dynamic balance where accumulation stops.

The required throughput to be pumped for each species, based on the particle flow rate from the plasma side, is given by:

$$Q_{x_{div}} = \dot{N}_{x_{div}} k_B T$$

Where $T = 273\ \text{K}$

The actual throughput handled by the vacuum pumping system is computed as the sum over all active pumps:

$$Q_{x,VP} = \sum_{j=1}^{n_{pumps}} p_x S_{x,j} \varphi_j$$

The rate of change of partial pressure for species x inside the divertor volume is then given by:

$$\frac{\partial p_x}{\partial t} = \frac{Q_{x_{div}} - Q_{x,VP}}{V_{div}}$$

This formulation allows for a time-dependent update of local pressure values in the divertor and leads to a self-consistent estimate of the number of active pumps required at each time step.

To estimate the divertor volume V_{div}, the tokamak is conceptually divided into two main regions:

1. The high-pressure, magnetically confined plasma core.
2. The remaining vessel volume, which includes the divertor plenum and other peripheral regions.

Assuming approximate volumes:

$$V_{TOKAMAK} \approx 1400\mathrm{m}^3;\ V_{PLASMA} \approx 840\mathrm{m}^3$$

$$V_{div} = V_{TOKAMAK} - V_{PLASMA} \approx 1400\mathrm{m}^3 - 840\mathrm{m}^3 = 560\mathrm{m}^3$$

For compact reactors volumes can be sensible smaller. Further discussions are provided on the results chapter.

When dynamic equilibrium will be reached, the condition

$$Q_{x_{div}} = Q_{x_{VP}}$$

will be satisfied, meaning that the rate at which a species enters the divertor equals the rate at which it is pumped out. As a result, the partial pressure of that species will stabilize and no further accumulation will occur.

3.4.3 Vacuum condition between pulse

A secondary but essential function of the vacuum pumping system is to re-establish ultra-high vacuum conditions in the reactor chamber before the start of a new plasma pulse.

This work includes a verification step to ensure that the number of pumps—along with their hierarchical regeneration strategy—is sufficient to achieve this requirement. The results demonstrate that the limiting constraint in pump sizing is actually the during-operation throughput, while the between-pulse evacuation is easily handled by the system.

To model the pump-down phase, we consider the gas input from the plasma to be zero, as expected during off-pulse conditions. The goal now is to evacuate the entire chamber volume, and the process can be described by the following differential equation:

$$\frac{\partial p}{\partial t} = -\frac{Q_{VP}}{V_{TOKAMAK}} = -\frac{pS_{VP}}{V_{TOKAMAK}}$$

With the initial and final conditions:

$$p(t = 0) = 3\mathrm{Pa}$$

$$p(t = t_{end}) = 10^{-6}\mathrm{Pa}$$

Neglecting, for simplicity, the time needed to regenerate the pumps, this equation can be solved analytically for the time required to reach the desired vacuum level. Assuming a single active pump with a nominal pumping speed of $S_{VP} = 60\mathrm{m}^3\mathrm{s}^{-1}$, and a tokamak volume of $V_{TOKAMAK} = 1400\ m^3$, we obtain:

$$t_{end} = \frac{\ln\left(\frac{p(0)}{p(t_{end})}\right) V_{TOKAMAK}}{S_{VP}} = 348\ [s] \sim 6\ [\mathrm{minutes}]$$

Alternatively, the equation can be solved for S_{VP} to determine the pumping speed required to achieve vacuum within a fixed time window.

Alternatively, the numerical solution for the evacuation time can be computed by the code using a fixed number of pumps—determined under pulse-on conditions—while also accounting for the previously discussed regeneration strategy. The results of this analysis will be presented in the next chapter.

Chapter 4 – Results and discussion

This chapter presents the simulation results obtained using the developed numerical model for the cryopumping system integrated into the fuel cycle of a nuclear fusion reactor. The model evaluates the required number of cryopumps based on reactor thermal power, tokamak and plasma geometries, and plasma performance assumptions. The results are discussed for three representative reactor concepts: an ITER-like reactor, a compact ARC-like reactor using high-temperature superconductors, and a DEMO-scale reactor.

4.1 Reactors parameters and configuration

The code was used to simulate three reactor scenarios, which differ in size, power, and design philosophy, summarized in Table 3 - Three reactor scenarios analysed in this work, with diverse power and sizes..

Table 3 - Three reactor scenarios analysed in this work, with diverse power and sizes.

Reactor	$P_{fus}[\mathrm{MW}]$	$V_{TOKAMAK}[\mathrm{m}^3]$	$V_{PLASMA}[\mathrm{m}^3]$	$V_{DIV}[\mathrm{m}^3]$	$P_{SOL}[\mathrm{MW}]$	$A_{DIV}[\mathrm{m}^2]$
ITER	500	1400	840	560	100	10
ARC	1000	230	140	90	200	20
DEMO	2000	4200	2500	1700	400	40

Where:

- P_{fus}: nominal thermal power of the reactor. It refers exclusively to the power generated by fusion reactions in the plasma. Any additional heat generated by neutron-induced fission in the breeding blanket is not included.
- $V_{TOKAMAK}$: internal vacuum vessel volume.
- V_{PLASMA}: plasma core volume.
- V_{DIV}: divertor region volume (estimated as the residual vessel volume after subtracting the plasma volume).
- P_{SOL}: estimated power flowing through the Scrape-Off Layer (assumed as 20% of total thermal power).
- A_{DIV}: divertor surface area being hit by the plasma exhaust

4.2 Divertor flow rates

The particle flow rate through the divertor is a key parameter for the design of the vacuum system, as it directly impacts the required pumping speed and the capacity of cryopumps. In this section, the gas throughput is evaluated for different fuelling strategies and isotopic compositions of the injected fuel, with particular focus on an ITER-like reactor configuration.

Simulations were performed under varying assumptions regarding the isotopic mix of the injected gas, which affects the effective neutral particle flux, and consequently the exhaust

load on the pumping system. In the reference case, a nominal fuelling composition of 50% D_2 and 50% T_2 was considered. Additionally, a tritium-lean mixture (e.g., 66% D_2 and 33% T_2) was studied to reflect scenarios where tritium availability is limited, such as during initial reactor start-up or in early campaigns of DEMO-like devices. Results are shown in Figure 29.

By fixing the tritium burning efficiency as an input parameter — thus neglecting the potential benefits that a tritium-lean mixture could have on improving it — the presence of additional deuterium leads to an increased neutral particle flux toward the divertor. This has direct implications for the pumping system, particularly in terms of hydrogen inventory management.

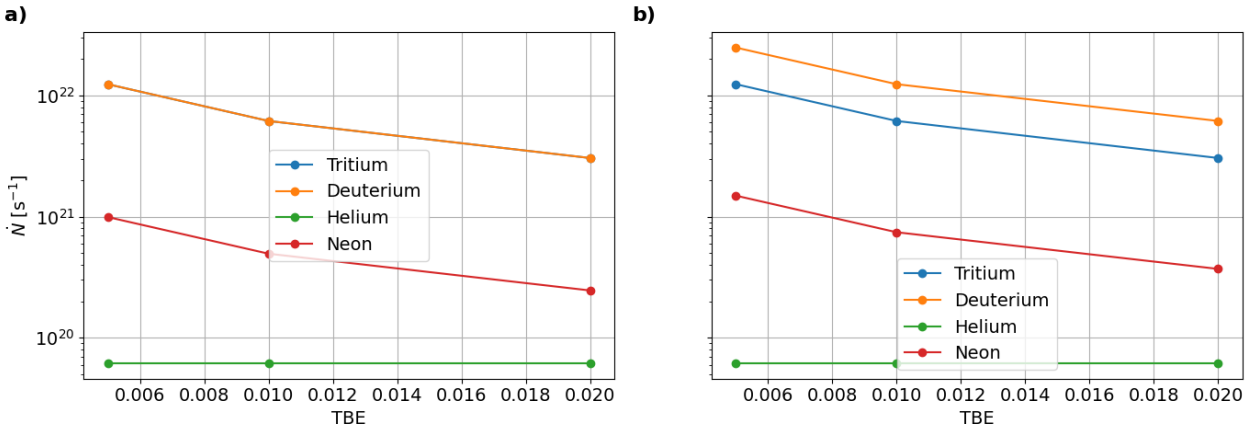

Figure 29 - Particle flow rates on an ITER-kind reactor for: a) Nominal fuelling strategy $k_{DTin} = 1$ (50% D_2, 50% T_2); b) Tritium-lean fuelling strategy $k_{DTin} = 2$ (66% D_2, 33% T_2).

4.3 Divertor Pressure and Density results

Results are shown for both analytic and numerical method.

4.3.1 Physics-based analytic method

In the analytical approach, the divertor pressure and neutral gas density are calculated based on simplified assumptions that enable closed-form expressions. One key result of this method is that the computed values remain invariant with respect to the reactor's nominal thermal power. This behaviour arises from the assumption that, although the particle flux increases linearly with the fusion power, the divertor area exhausting the thermal flux scales proportionally.

Specifically, the divertor surface area is defined based on the power that must be exhausted through the Scrape-Off Layer (SOL), which is assumed to be a fixed fraction of the total thermal power of the plasma:

$$P_{SOL} = \frac{P_{fus}}{5} \text{ [MW]}$$

As a result, the particle flux per unit area of the divertor remains constant across reactors of different sizes or power levels. This leads to unchanged values of divertor neutral pressure and density, under the assumptions of the model.

The results also indicate a decreasing trend in the partial pressure and neutral density for all gas species except helium, which remains constant. This behaviour is illustrated in Figure 30 and is directly related to the fact that helium production originates from the fusion reactions and is independent of the tritium burning efficiency.

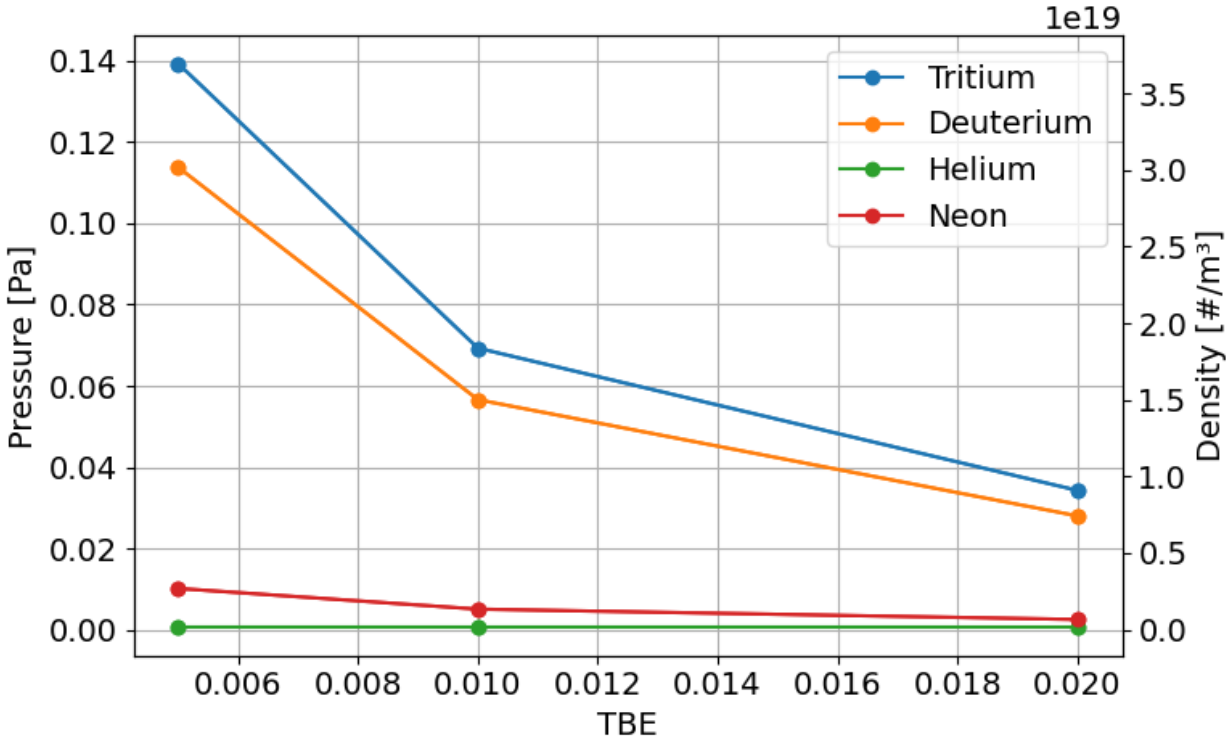

Figure 30 - Analytic calculations for divertor pressure and density for the ITER-kind reactor with nominal fuelling strategy

It is important to note that the analytic method underestimates the pressure and density in the pumping region when compared to more detailed numerical simulations. This discrepancy is primarily due to the simplified nature of the analytical model, which does not account for transport phenomena and geometry-dependent factors.

4.3.2 Numerical iterative method

The numerical iterative method was applied to three different reactor configurations: an ITER-like reactor, a compact ARC-type reactor, and a DEMO-scale reactor. Each design is characterized by a distinct nominal thermal power and divertor volume, which significantly

influence the resulting neutral gas pressure in the pumping region. The comparison in shown in Figure 31.

The results show clear differences in divertor pressure levels among the three configurations:

- The compact reactor (ARC-like) exhibits the highest divertor pressure, primarily due to its small vessel volume combined with a moderate power level. The reduced volume limits the neutral expansion and contributes to higher local gas densities.
- In contrast, the ITER-like reactor shows the lowest pressure values, which can be attributed to its large vessel volume and relatively lower thermal power. The larger space allows for better neutral dispersion, thus reducing local pressure.
- The DEMO-scale reactor presents intermediate pressure values, which fall within the typical expected range of 1 to 10 Pa in the pumping region.
- Thesis results align well with experimental design expectations for future fusion reactors and suggests that those reactors could operate near expected conditions for cryopumping performance.

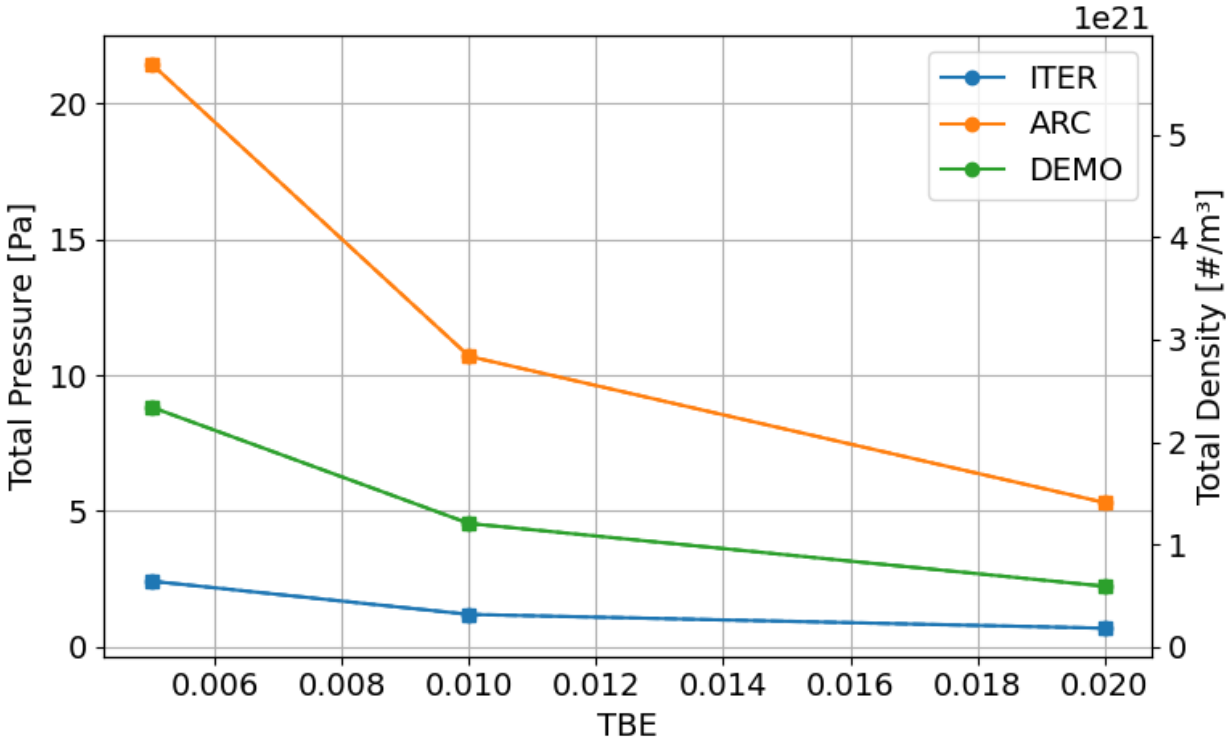

Figure 31 – Total pressure and density in the pumping volume for different reactors vs TBE

The Figure 32 presents the species-resolved pressure distribution for a single reactor configuration, illustrating the contribution of each gas species to the total divertor pressure. As an example, results for the DEMO reactor are shown in Figure 32, highlighting the relatively dominant presence of hydrogen isotopes, and the relatively low presence of helium ash and

neon impurities in the pumping region.

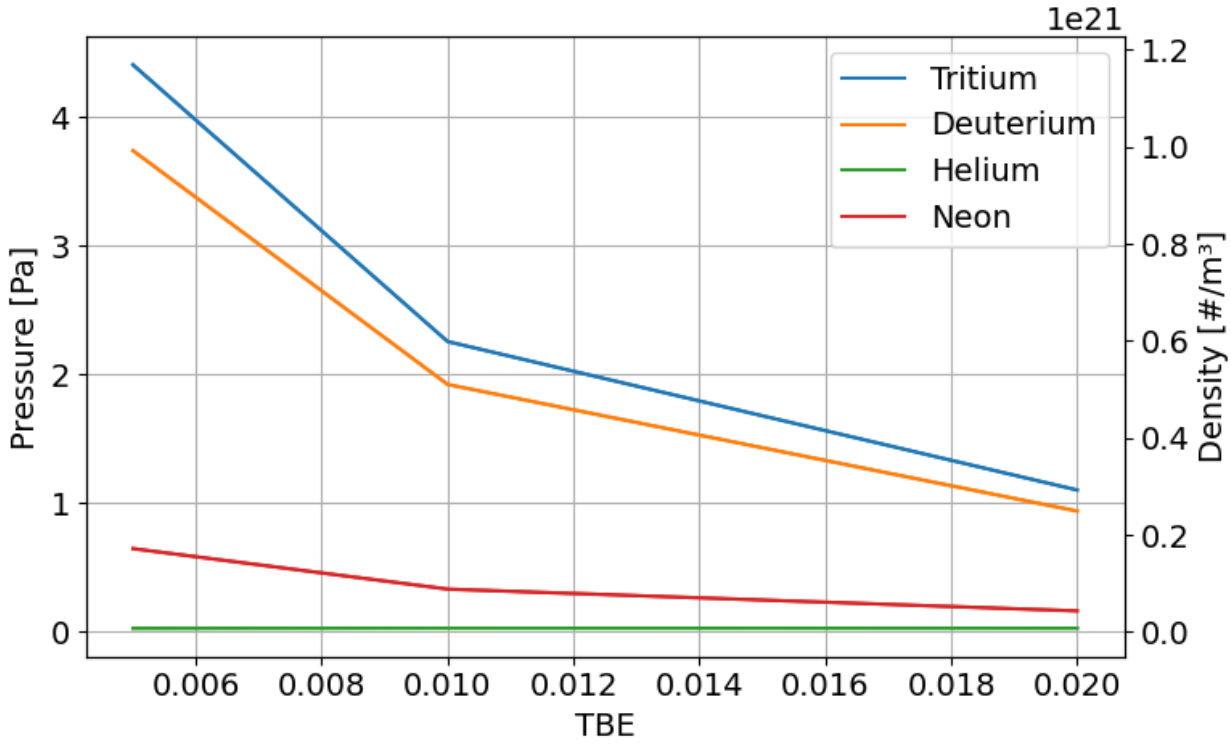

Figure 32 - Species partial pressure distribution for DEMO-scale reactor with different TBE

4.4 Number of pumps

The estimated number of required cryopumps was evaluated for each reactor configuration, based on the computed gas flow rates and the assumed tritium burning efficiency (Figure 33).

For the ITER-like reactor, the required number of pumps is consistent with existing design expectations. ITER is designed to operate with a TBE in the range of 0.005 to 0.01, and its current baseline configuration includes six torus cryopumps. The results obtained through the model align with this design, confirming the validity of the computational approach for ITER-scale systems.

For the compact ARC-type reactor, the model predicts a need for approximately five pumps, assuming a TBE of 0.02. While this expected TBE value is higher than the ITER's one, it is compatible with the more advanced plasma performance expected in high-field compact reactors. Although space constraints are more severe in ARC due to its reduced size, the number of pumps remains reasonable. It also suggests that potentially smaller-sized high-performance cryopumps could better meet the design requirements.

In the case of DEMO, the largest reactor considered in this study, the estimated number of required pumps is significantly higher. This is due to the combination of a high nominal fusion thermal power and large divertor exhaust volumes, which result in substantial gas loads. The analysis suggests that the use of larger cryopumps with enhanced capacity and higher effective pumping speeds could be necessary. Feasibility should be verified since number of pumps

depends strongly on TBE. A low TBE could lead to an excessively high number of pumps, potentially causing spatial constraints both inside the vacuum chamber and in the auxiliary buildings.

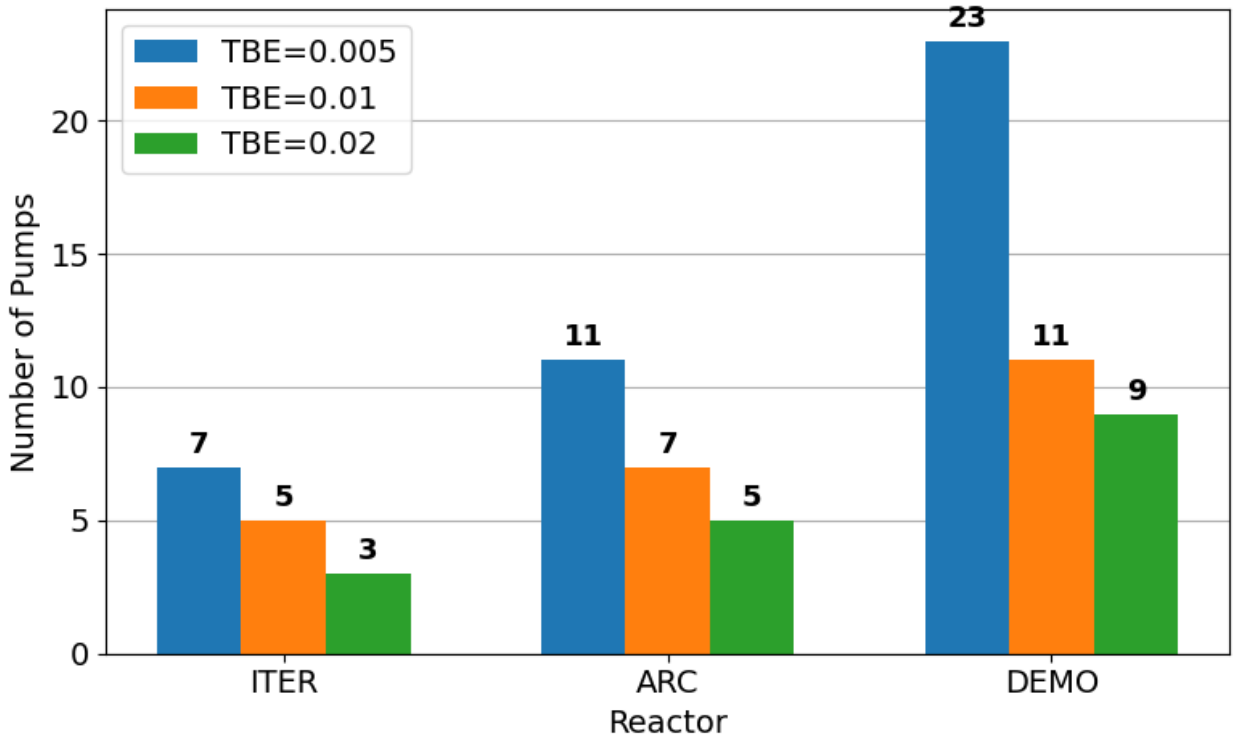

Figure 33 - Required number of pumps mounted in the VP for different reactors and different TBE

4.5 Tritium inventory startup

In this section the tritium inventory required for the startup of the different reactors is computed and shown in Figure 34.

As expected, the initial tritium inventory required for reactor startup $I_{startup}$ increases with the reactor's nominal fusion power. Among the three designs analysed, the DEMO reactor—being the one with the highest P_{fus} —requires the largest quantity of tritium to initiate operations. In the worst-case scenario considered in the simulations, the startup demand exceeds 20 kilograms of tritium.

This requirement is particularly concerning, as it represents a significant fraction of the current global tritium inventory, which is estimated to be around 30-40 kg [24]. Such a high initial demand poses a serious bottleneck for the deployment of large-scale fusion power, especially during the early phases of reactor commissioning and ramp-up. In this context, strategies

aimed at increasing plasma performance, and enhancing the tritium burning efficiency (TBE), could lead to substantial reductions in $I_{startup}$ and mitigate the associated supply challenges.

It is important to highlight that in these simulations, the Tritium Breeding Ratio was set to TBR = 1.073. This value is consistent with recent estimates for advanced breeding blanket concepts and reflects a realistic assumption for future fusion systems.

In contrast, lower-power reactors such as ARC and ITER require significantly smaller startup inventories, in the range of a few kilograms. The trend observed suggests an approximately linear correlation between nominal fusion power and $I_{startup}$. On the other hand, the reactor size (i.e., vessel or plasma volume) appears to have a limited influence on $I_{startup}$. However, it should be noted that tritium trapping is not considered in this model. Tritium trapping strongly depends on breeding blanket and vacuum vessel volumes, as well as tritium-facing surfaces. Preliminary results suggest that when tritium trapping is included in fuel cycle models, the startup inventory increases non-linearly with those quantities, thus introducing also a dependency of $I_{startup}$ on them [25].

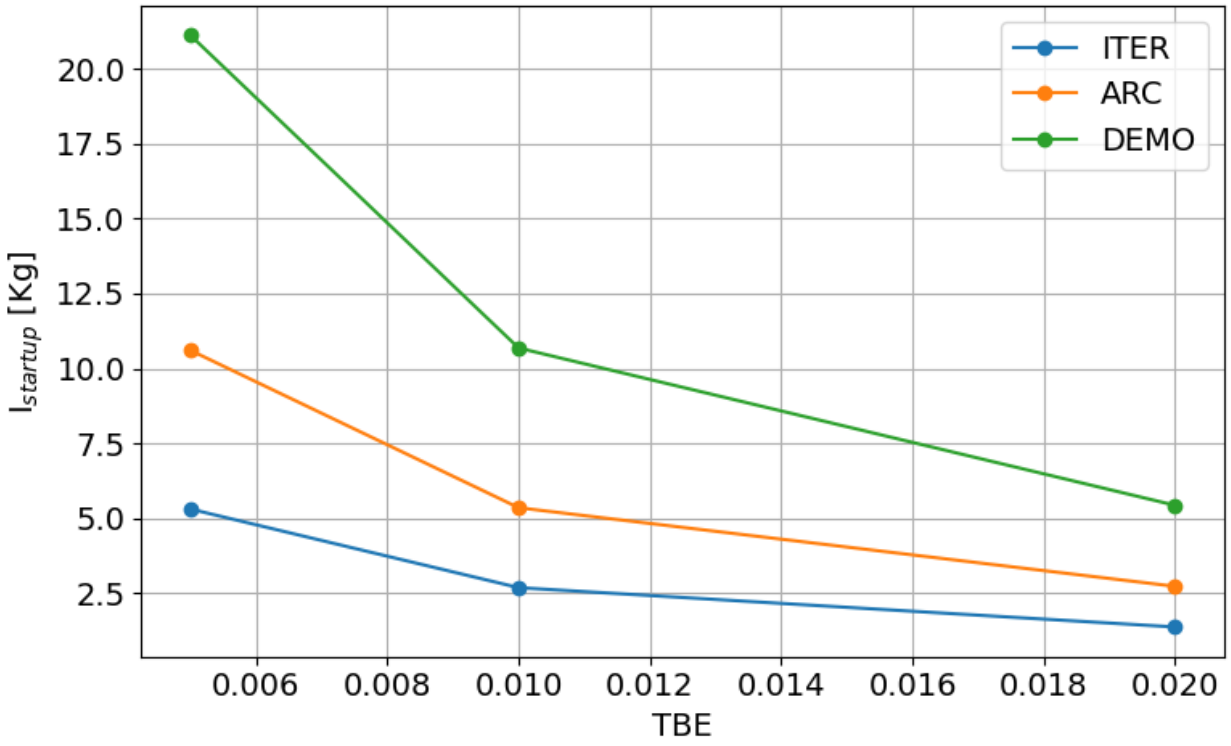

Figure 34 - Tritium inventory startup required for different reactors with different power levels against expected TBE

4.6 Pumps inventory

The gas inventory of each cryopump evolves over time according to the divertor gas flow rates and the maximum throughput capacity of the pump. As neutral particles are continuously pumped from the divertor region, gases gradually accumulate on the cryosorbing surfaces of the pump, and their presence must be carefully monitored to avoid exceeding operational safety limits.

The most common trigger for partial regeneration is reaching the hydrogen explosion threshold, which represents a critical limit for the safe operation of the cryopumping system. Once this threshold is reached, the affected pump must temporarily suspend operation and undergo partial regeneration: during this phase, the accumulated gases (primarily hydrogen isotopes and helium) are evaporated and desorbed, allowing them to be extracted by a forepump system and safely removed from the cryopump chamber.

However, water-like species (including water vapor, ammonia, and other oxidized compounds) do not desorb effectively at cryogenic temperatures around 90 K. These species continue to accumulate in the chamber over time and can only be removed during high-temperature (full) regeneration cycles, which are more invasive and time-consuming. In simulations using a tritium-lean fuelling mixture (66% deuterium, 33% tritium), and under ITER-like reactor conditions, it was found that the water-species saturation limit is reached after approximately 31 hours of continuous operation, necessitating full regeneration at that point (Figure 35).

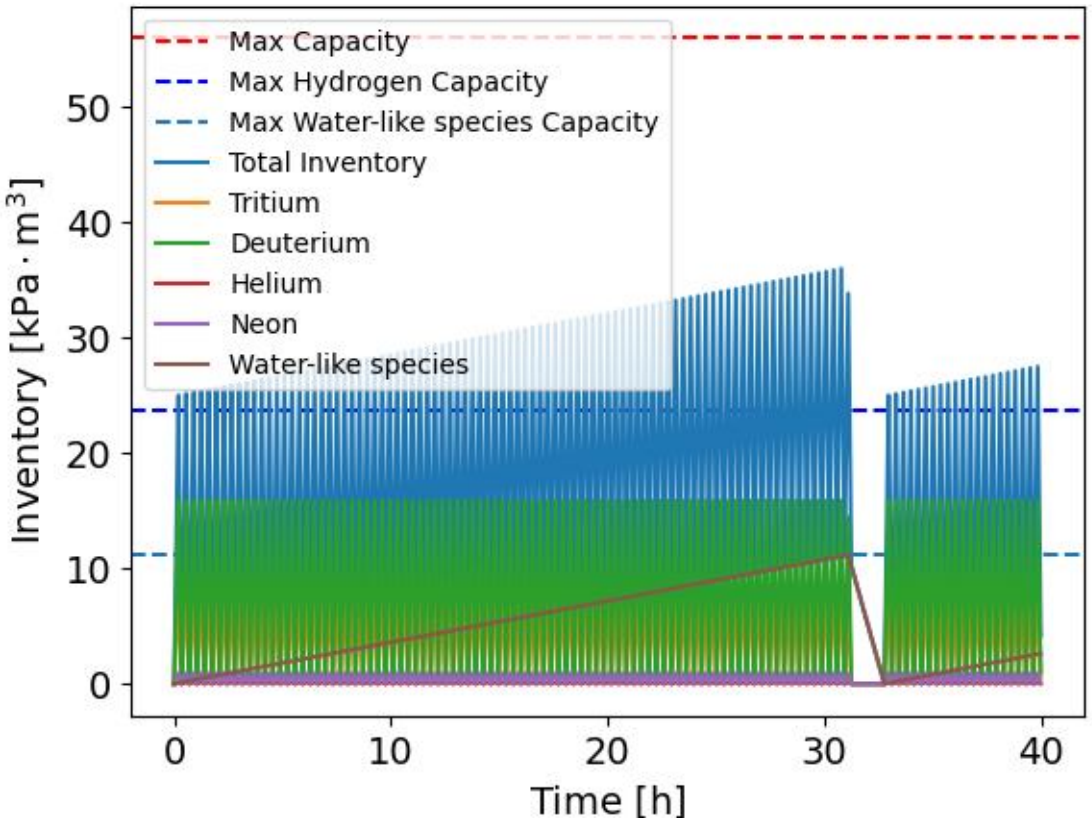

Figure 35 - Main pump (pump n.1) gas inventory divided in each internal specie inventory. High-temperature regeneration appears to be required after 31h of operation and after several cicles of adsorption and partial regeneration of the surfaces.

The dynamic behaviour of the pumps also reflects the hierarchical control strategy implemented in the simulation. For example, in the scenario analysed in Figure 36, Pump 2 never independently reaches the hydrogen inventory threshold. Instead, it undergoes partial regeneration simply because Pump 1 completes its own regeneration cycle and becomes

available again. This coordinated behaviour ensures continuous operation of the pumping system by alternating regeneration cycles, preventing total system shutdowns.

Additionally, the simulation shows that when Pump 2 re-enters operation, it initially handles only a fraction of the incoming flow. This is managed by partially closing its inlet valve, so that Pump 2 functions primarily as a support unit to Pump 1. This is particularly important because, after prolonged operation, Pump 1 begins to approach its saturation limit, causing a reduction in its effective pumping speed. This strategy ensures that pumping performance is maintained over time while staying within safe operational margins.

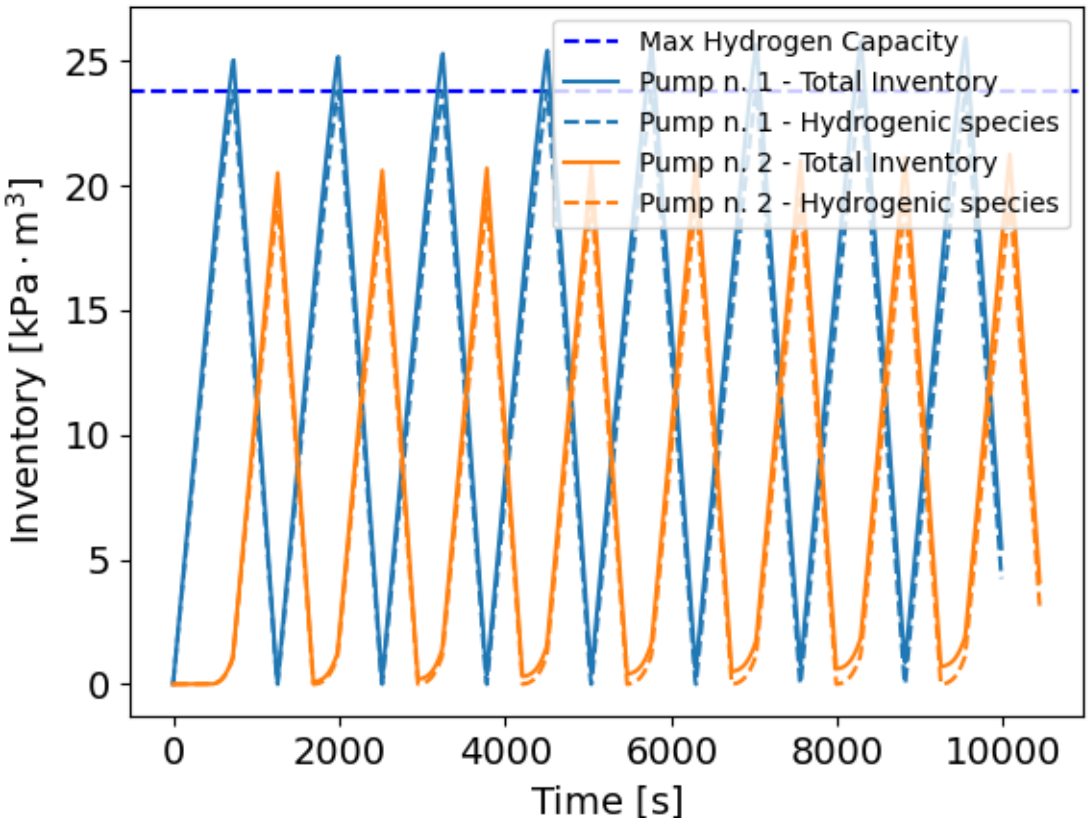

Figure 36 - Vacuum pumps dynamic behaviour and interaction. Hierarchical control is shown. Pump n.1 is the main pump and activates as soon as it is available. Pump n.2 support Pump n.1, when it undergoes regeneration or its pumping speed is reduced because of surface saturation.

4.7 Pump down verification

A verification was conducted to assess the capability of the vacuum pumping system to reduce the vessel pressure to acceptable levels during the dwell time between pulses. This evaluation allows to rely on the system to return the reactor to operational vacuum conditions before each new plasma shot, without introducing delays in the pulse schedule.

Figure 37 displays the pressure decay profile for the ITER-like reactor. Under the worst-case scenario analysed (the case with highest TBE and, consequently, the minimum number of installed pumps (N_{pumps} = 3)), the system successfully reaches the target vacuum pressure of

10^{-6} Pa in 116 seconds, less than two minutes. This is fully compatible with the expected dwell time between pulses for ITER, confirming the adequacy of the vacuum system even under limiting conditions.

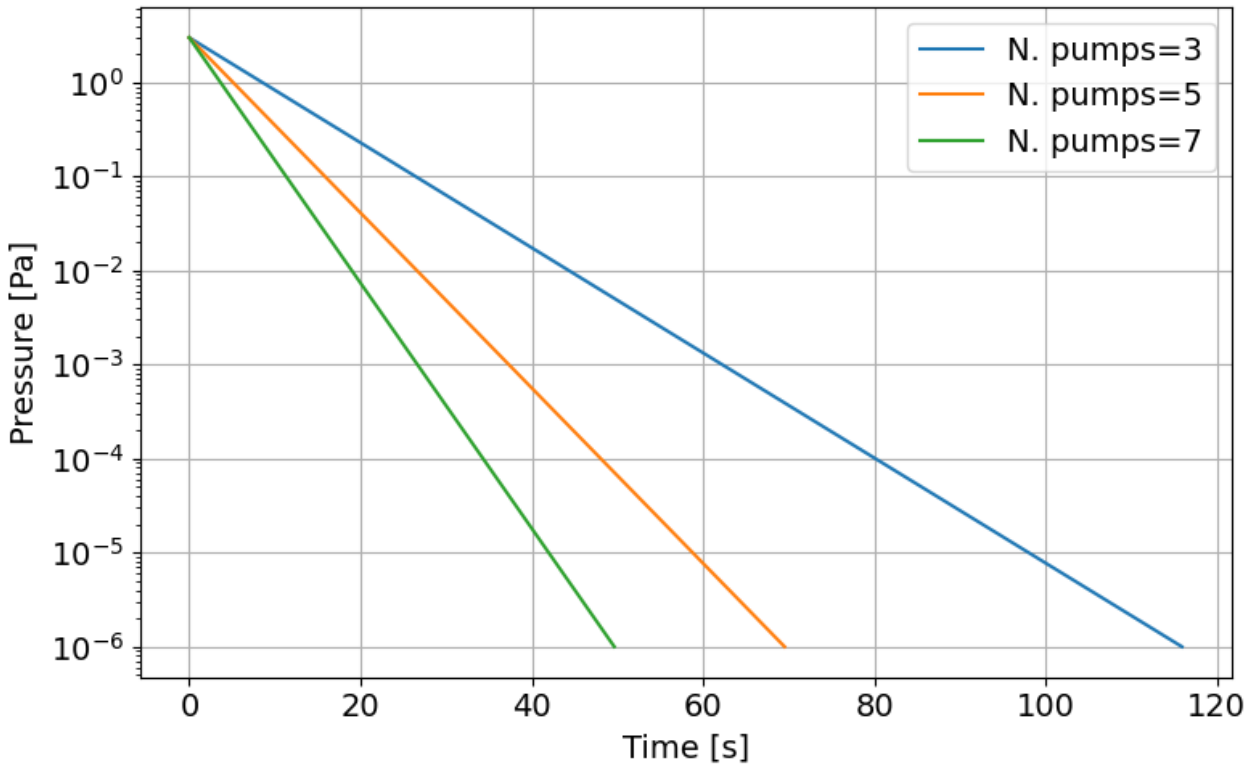

Figure 37 - Pressure vs time during dwell phase time. The required high-vacuum before starting a new pulse is set to be $10^{-6}Pa$.

Table 4 summarizes the pump-down performance for the three reactor configurations considered, exploring various pump configurations and vessel volumes. An internal pressure equal to 3 Pa is assumed after each pulse, and the target pressure between pulses has been set equal to 10^{-6}Pa.

Table 4 – Pump-down time for different reactors according to their different size.

Reactor	$V_{TOKAMAK}[\mathrm{m}^3]$	N_{pumps}	$t_{end}[\mathrm{s}]$
ITER	1400	3	115.9
ITER	1400	5	69.5
ITER	1400	7	49.6
ARC	230	5	4.4
ARC	230	7	3.1
ARC	230	11	2.0
DEMO	4200	9	115.9
DEMO	4200	11	94.8
DEMO	4200	23	45.3

These results show that:

- The ARC reactor, due to its small vacuum chamber volume, can be pumped down very rapidly, even with a modest number of pumps.
- The DEMO reactor, with its much larger volume, requires a correspondingly higher number of pumps to achieve fast pump-down. However, even for DEMO, a configuration with 9 pumps can reduce the pressure to operational vacuum in under 2 minutes, meeting the expected requirements.

4.8 Tritium inventory in the FC

Following the implementation of the new Vacuum Pumping (VP) component, the initial tritium inventory $I_{startup}$ required for reactor startup in a 500 MW test reactor remains essentially unchanged. This confirms that the upgraded pumping model does not significantly alter the global mass balance at startup conditions, which is primarily governed by plasma performance and tritium breeding parameters.

However, the dynamic redistribution of tritium throughout the Fuel Cycle is now more accurately represented in Figure 38. In particular, time-dependent inventories within the VP unit and its interconnected systems, such as the Fuel Cleanup System, show enhanced resolution and realism. This is illustrated in Figure 38, where the evolution of tritium content in each subsystem is plotted over time.

The improved model captures key transient behaviours, such as:

- The temporary retention and subsequent release of tritium during pump regeneration phases;
- The interaction with fuel cleanup loops, where tritium is recovered and redirected toward storage and reinjection.

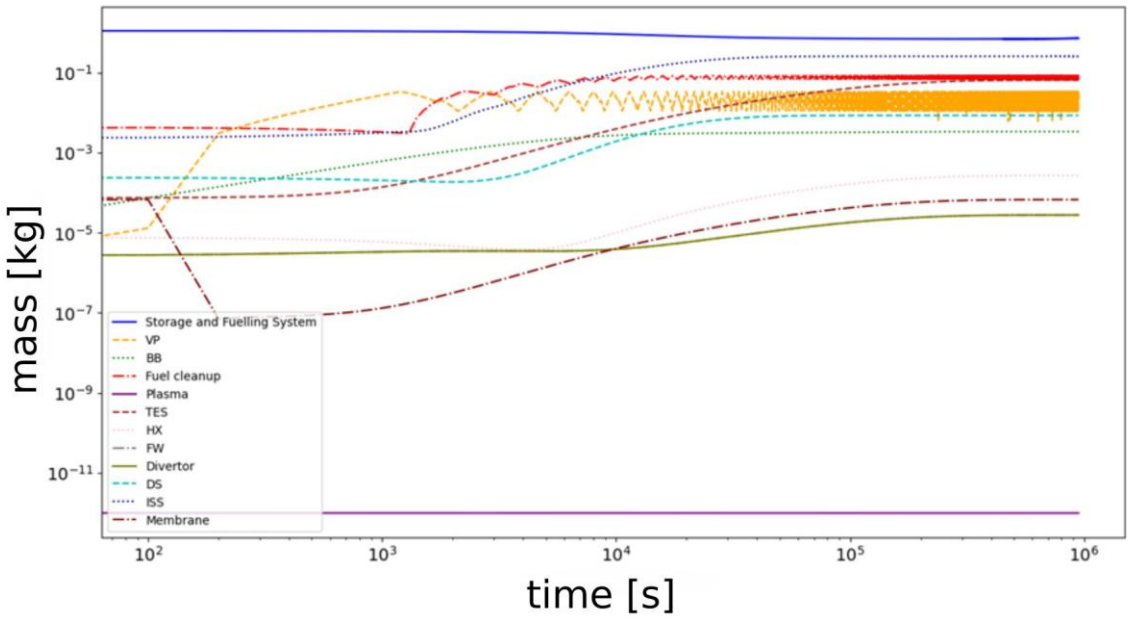

Figure 38 - Tritium inventories in the FC components with TBE = 0.02 after integration of the physics-based VP component

Chapter 5 - Conclusions

This thesis presents a numerical model of the dynamic behaviour of vacuum pumping systems. This model has been integrated into the existing fuel cycle model.

The aim was to determine the minimum number of pumps required for the vacuum pumping system to ensure tritium self-sufficiency while maintaining nominal reactor operation. This approach enables the dynamic representation of gas inventory evolution and surface saturation in the cryopump.

The results are consistent with the current design of the ITER vacuum pumping system, which includes six torus cryopumps. Depending on the expected TBE, the model predicts a number between five and seven pumps. The model was then applied to ARC and DEMO-like reactors, with the results showing a higher number of pumps, suggesting the need for pumps with increased dimensions and capacity.

The created model is physics-based and includes dynamic pumping speed and the physical limitation of the pump's capacity. However, due to a lack of data and the complexity of modelling, some hypotheses have been put forward that limit the model and could be improved in future versions.

Hypotheses regarding the regeneration time required for both partial and total regeneration limit the depth of the analysis. Further modelling efforts could be employed to model the internal pressure of the chamber and the charcoal surface temperature, enabling a more accurate characterisation of evaporation and desorption speeds. Furthermore, optimising the frequency of high-temperature regeneration would allow for a more efficient use of the installed pumps and improve the current hierarchical strategy.

Future work will study the energy required for cooling in the regeneration phase and set this as a minimisation requirement, enabling the model to compare different regeneration strategies and look for a balance between minimising mounted pumps and cooling energy. Also, realistic simulations of a direct internal recycling system including species-dependent dynamics might be carried out with the current models.

In its current configuration, the model can be used in the initial design phase of a nuclear fusion reactor to estimate the required number of pumps and the operating time before regeneration, as well as considering variable and transient D-T mixtures. Input parameters include the nominal fusion power of the plant, the chamber volume and the expected tritium burning efficiency.

Bibliography

[1] S. Meschini, S. E. Ferry, R. Delaporte-Mathurin, and D. G. Whyte, "Modeling and analysis of the tritium fuel cycle for ARC- and STEP-class D-T fusion power plants," *Nucl. Fusion*, vol. 63, no. 12, p. 126005, Dec. 2023, doi: 10.1088/1741-4326/acf3fc.

[2] J. F. Parisi, S. Meschini, A. Rutkowski, and A. Diallo, "Tritium-Lean Fusion Power Plants with Asymmetric Deuterium-Tritium Transport and Pumping," 2024, *arXiv*. doi: 10.48550/ARXIV.2410.05238.

[3] F. Subba, D. P. Coster, M. Moscheni, and M. Siccinio, "SOLPS-ITER modeling of divertor scenarios for EU-DEMO," *Nucl. Fusion*, vol. 61, no. 10, p. 106013, Oct. 2021, doi: 10.1088/1741-4326/ac1c85.

[4] *Fundamentals of Magnetic Fusion Technology*. in Non-serial Publications. Vienna: INTERNATIONAL ATOMIC ENERGY AGENCY, 2023. [Online]. Available: https://www.iaea.org/publications/14898/fundamentals-of-magnetic-fusion-technology

[5] R. J. Pearce *et al.*, "The ITER divertor pumping system, design evolution, simplification and performance," *Fusion Engineering and Design*, vol. 88, no. 6–8, pp. 809–813, Oct. 2013, doi: 10.1016/j.fusengdes.2013.01.050.

[6] C. Day, "Basics and Applications of Cryopumps," *CAS 2006 - CERN Accelerator School: Vacuum in Accelerators, Proceedings*, Jan. 2006.

[7] C. Gleason-González, S. Varoutis, V. Hauer, and C. Day, "Simulation of neutral gas flow in a tokamak divertor using the Direct Simulation Monte Carlo method," *Fusion Engineering and Design*, vol. 89, no. 7–8, pp. 1042–1047, Oct. 2014, doi: 10.1016/j.fusengdes.2014.02.005.

[8] M. Dremel *et al.*, "The new build to print design of the ITER Torus Cryopump," *Fusion Engineering and Design*, vol. 88, no. 6–8, pp. 760–763, Oct. 2013, doi: 10.1016/j.fusengdes.2013.02.026.

[9] "CSIC Pride Cryogenics." Accessed: Jun. 05, 2025. [Online]. Available: https://www.724pridecryogenics.com/en/product5.asp?bigid=109

[10] S. Varoutis *et al.*, "Simulation of neutral gas flow in the JET sub-divertor," *Fusion Engineering and Design*, vol. 121, pp. 13–21, Oct. 2017, doi: 10.1016/j.fusengdes.2017.05.108.

[11] X. Luo, C. Day, H. Haas, and S. Varoutis, "Experimental results and numerical modeling of a high-performance large-scale cryopump. I. Test particle Monte Carlo simulation," *Journal of Vacuum Science & Technology A: Vacuum, Surfaces, and Films*, vol. 29, no. 4, p. 041601, Jul. 2011, doi: 10.1116/1.3585665.

[12] "lect_day."

[13] C. Day, B. Kammerer, and A. Mack, "The influence of water on the performance of ITER cryosorption vacuum pumps," *Fusion Engineering and Design*, vol. 51–52, pp. 229–235, Nov. 2000, doi: 10.1016/S0920-3796(00)00322-7.

[14] C. Day, A. Antipenkov, M. Dremel, H. Haas, V. Hauer, and A. Mack, "Validated Design of the ITER Main Vacuum Pumping Systems".

[15] Y. Zhou, H. Feng, S. Zhang, M. Zhuang, and Z. Zhao, "Design and Analysis of the Inlet Valve for the CFETR Torus Cryopump," *Energies*, vol. 16, no. 7, p. 3107, Mar. 2023, doi: 10.3390/en16073107.

[16] C. Day, "USE OF POROUS MATERIALS FOR CRYOPUMPING," in *Handbook of Surfaces and Interfaces of Materials*, Elsevier, 2001, pp. 265–307. doi: 10.1016/B978-012513910-6/50065-7.

[17] C. Day *et al.*, “Hydrogen inventories in the vacuum pumping systems of ITER,” *Fusion Engineering and Design*, vol. 81, no. 1–7, pp. 777–784, Feb. 2006, doi: 10.1016/j.fusengdes.2005.07.020.
[18] Chr. Day and H. Haas, “Experimental assessment of the ITER cryosorption pump high temperature regeneration,” *Fusion Engineering and Design*, vol. 84, no. 2–6, pp. 665–668, Jun. 2009, doi: 10.1016/j.fusengdes.2009.02.018.
[19] T. Giegerich and C. Day, “The KALPUREX-process – A new vacuum pumping process for exhaust gases in fusion power plants,” *Fusion Engineering and Design*, vol. 89, no. 7–8, pp. 1476–1481, Oct. 2014, doi: 10.1016/j.fusengdes.2014.03.082.
[20] “√ Diffusion pumps.” Accessed: Jun. 08, 2025. [Online]. Available: https://www.alcatechnology.com/en/blog/diffusion-pumps/
[21] R. J. H. Pearce *et al.*, “Gas species, their evolution and segregation through the ITER vacuum systems,” *Vacuum*, vol. 86, no. 11, pp. 1725–1730, May 2012, doi: 10.1016/j.vacuum.2012.03.048.
[22] E. Serra, R. J. Ciora, D. De Meis, and M. Richetta, “Plasma enhancement gases (PEGs) separation using a carbon molecular sieve (CMS) membrane,” *Fusion Engineering and Design*, vol. 146, pp. 2438–2441, Sep. 2019, doi: 10.1016/j.fusengdes.2019.04.013.
[23] A. Zito *et al.*, “SOLPS-ITER modelling of helium transport, recycling and pumping at the ASDEX Upgrade tokamak,” *Nucl. Fusion*, vol. 65, no. 4, p. 046022, Apr. 2025, doi: 10.1088/1741-4326/adbe90.
[24] “Tritium resources available for fusion reactors - IOPscience.” Accessed: Jun. 18, 2025. [Online]. Available: https://iopscience.iop.org/article/10.1088/1741-4326/aa9d25/meta
[25] S. Meschini, R. Delaporte-Mathurin, G. R. Tynan, and S. E. Ferry, “Impact of trapping on tritium self-sufficiency and tritium inventories in fusion power plant fuel cycles,” *Nucl. Fusion*, vol. 65, no. 3, p. 036010, Mar. 2025, doi: 10.1088/1741-4326/adacfa.